

# LOAN DOCUMENT

PHOTOGRAPH THIS SHEET

AD-A277 487



DTIC ACCESSION NUMBER

LEVEL

①

INVENTORY

WL-Tm-94-3031

DOCUMENT IDENTIFICATION

Feb 94

Approved for public release  
Distribution Unlimited

DISTRIBUTION STATEMENT

DTIC ACCESSION NUMBER	
NTIS	GRA&I
DTIC	TRAC
UNANNOUNCED	
JUSTIFICATION	
BY	
DISTRIBUTION/	
AVAILABILITY CODES	
DISTRIBUTION	AVAILABILITY AND/OR SPECIAL
A-1	

DISTRIBUTION STAMP

**DTIC**  
ELECTE  
MAR 29 1994  
**C D**

DATE ACCESSIONED

DATE RETURNED

94 3 24 062

DATE RECEIVED IN DTIC

REGISTERED OR CERTIFIED NUMBER

PHOTOGRAPH THIS SHEET AND RETURN TO DTIC-FDAC

H  
A  
N  
D  
L  
E  
W  
I  
T  
H  
C  
A  
R  
E

**AD-A277 487**



WL-TM-94-3031



# **RESPONSE OF A CANTILEVERED PLATE IN SUPERSONIC FLOW**

**Mark A. Hopkins**

**Structural Dynamics Branch  
Structures Division**

**February 1994**

**Interim Report for period January 1993 - February 1994**


Approved for public release; distribution is unlimited.

DTIC QUALITY INSPECTED 1

**Flight Dynamics Directorate  
Wright Laboratory  
Air Force Materiel Command  
Wright-Patterson Air Force Base, Ohio 45433-7552**

## FOREWORD

This work was prepared by personnel in the Aeroelasticity Section, Structural Dynamics Branch of the Structures Division in the Flight Dynamics Directorate. The effort reported herein was conducted under Work Units 24010800, "Aeroelasticity," and 2302AW01, "Vibration Suppression." This manuscript was released in February 1994 for publication as a Technical Memorandum and covers work conducted from January 1993 to February 1994.



MARK A. HOPKINS  
Aerospace Engineer  
Aeroelasticity Section

This memorandum has been reviewed and approved.



TERRY M. HARRIS  
Technical Manager, Aeroelasticity Section  
Structural Dynamics Branch



JOSEPH W. MOSCHLER  
Chief, Structural Dynamics Branch  
Structures Division

REPORT DOCUMENTATION PAGE			Form Approved OMB No. 0704-0188	
<small>Public reporting burden for this collection of information is estimated to average 1 hour per response, including the time for reviewing existing data sources, gathering and maintaining the data needed, and completing and reviewing the collection of information. Send comments regarding this burden estimate or any other aspect of this collection of information, including suggestions for reducing the burden, to Washington Headquarters Service, Paperwork Project (0704-0188), Washington, DC 20503.</small>				
1. AGENCY USE ONLY (Leave blank)		2. REPORT DATE <b>February 1994</b>		3. REPORT TYPE AND DATES COVERED <b>Interim Report, January 1993 - February 1994</b>
4. TITLE AND SUBTITLE <b>Response of a Cantilevered Plate in Supersonic Flow</b>			5. FUNDING NUMBERS <b>PE: 62201F PR: 2401 TA: 08 WU: 00</b>	
6. AUTHOR(S) <b>Mark A. Hopkins</b>				
7. PERFORMING ORGANIZATION NAME(S) AND ADDRESS(ES) <b>Structural Dynamics Branch Structures Division Flight Dynamics Directorate Wright Laboratory Wright-Patterson Air Force Base, OH 45433-7552</b>			8. PERFORMING ORGANIZATION REPORT NUMBER <b>WL-TM-94-3031</b>	
9. SPONSORING / MONITORING AGENCY NAME(S) AND ADDRESS(ES) <b>FLIGHT DYNAMICS DIRECTORATE WRIGHT LABORATORY AIR FORCE MATERIEL COMMAND WRIGHT PATTERSON AFB OH 45433-7562</b>			10. SPONSORING / MONITORING AGENCY REPORT NUMBER <b>WL-TM-94-3031</b>	
11. SUPPLEMENTARY NOTES				
12a. DISTRIBUTION / AVAILABILITY STATEMENT <b>Approved for public release; distribution is unlimited.</b>			12b. DISTRIBUTION CODE	
13. ABSTRACT (Maximum 200 words) <p>The response of a thin rectangular panel to supersonic flow over its upper surface is investigated. The panel is fabricated of an isotropic material and has a constant thickness. The panel is fixed along one side such that the flow passes over its freely supported leading and trailing edges parallel to the fixed edge. A Rayleigh-Ritz method is applied to determine the in-plane and transverse response of the panel. The panel deflections either decay to a zero equilibrium or grow to a limited amplitude oscillation once the transients have decayed depending on the panel and flow parameters. At some combination of panel and flow parameters, the panel will begin to oscillate harmonically about a buckled state. Further increasing the flow conditions will cause the panel to either oscillate periodically about a buckled state or nonperiodically. The steady state response is dependent on the flow conditions and the initial deflections and velocity profiles of the panel. The flow Mach number and panel length-to-width ratios were varied. the cantilevered panel response is compared to previous research. A simply supported panel is briefly discussed and its response is also compared to previous work.</p>				
14. SUBJECT TERMS <b>aeroelasticity, panel flutter, nonlinear dynamics</b>			15. NUMBER OF PAGES <b>52</b>	
			16. PRICE CODE	
17. SECURITY CLASSIFICATION OF REPORT <b>Unclassified</b>	18. SECURITY CLASSIFICATION OF THIS PAGE <b>Unclassified</b>	19. SECURITY CLASSIFICATION OF ABSTRACT <b>Unclassified</b>	20. LIMITATION OF ABSTRACT <b>UL</b>	

## TABLE OF CONTENTS

Section		Page
	Symbols .....	iv
I	Introduction .....	1
II	Analytical Procedure .....	2
III	Numerical Results .....	7
	Modal Convergence .....	7
	Structural Response .....	15
	Initial Condition Variation .....	34
IV	Comparison to Previous Research .....	41
V	Conclusions .....	45
VI	Acknowledgement .....	46
VII	Reference List .....	47

## SYMBOLS

### English Nomenclature

$a, b$	plate streamwise and spanwise lengths (or length and width)
$\bar{a}_{ij}, \bar{b}_{ij}, \bar{c}_{ij}$	nondimensional generalized coordinates in $x, y$ , and $z$ directions
$D$	plate bending stiffness
$E$	Young's modulus
$G$	shear modulus
$h$	plate thickness
$M_\infty$	freestream Mach number
$m_p = \rho_p h$	plate mass per unit area
$NXU, NXV, NXW$	number of assumed modes in $x$ direction defining $\bar{u}, \bar{v}$ , and $\bar{w}$
$NYU, NYV, NYW$	number of assumed modes in $y$ direction defining $\bar{u}, \bar{v}$ , and $\bar{w}$
$t$	time
$U_\infty$	freestream velocity
$\bar{u}, \bar{v}$	nondimensional in-plane displacements in $x$ and $y$ directions
$\bar{w}$	nondimensional transverse displacement measured from midplane
$x, y, z$	dimensional spacial coordinates
$\bar{x} = \frac{x}{a}, \bar{y} = \frac{y}{b}, \bar{z} = \frac{z}{h}$	nondimensional spacial coordinates

### Greek Nomenclature

$\beta = (M_\infty^2 - 1)^{1/2}$	compressibility correction factor
$\alpha_i, \beta_j$	in-plane modal functions in $x$ and $y$ directions
$\lambda = \rho_\infty U_\infty^2 a^3 D^{-1}$	nondimensional dynamic pressure
$\mu = \frac{\rho_\infty a}{\rho_p h}$	nondimensional mass ratio
$\nu$	Poisson's ratio
$\rho_\infty, \rho_p$	flow and plate mass densities
$\tau = t \left( \frac{m_p a^4}{D} \right)^{1/2}$	nondimensional time
$\phi_i, \psi_j$	transverse modal functions in $x$ and $y$ directions

## SUMMARY

The response of a thin rectangular panel to supersonic flow over its upper surface is investigated. The panel is fabricated of an isotropic material and has a constant thickness. The panel is fixed along one side such that the flow passes over its freely supported leading and trailing edges parallel to the fixed edge. A Rayleigh-Ritz method is applied to determine the in-plane and transverse response of the panel. The panel deflections either decay to a zero equilibrium or grow to a limited amplitude oscillation once the transients have decayed depending on the panel and flow parameters. At some combination of panel and flow parameters, the panel will begin to oscillate harmonically about a buckled state. Further increasing the flow conditions will cause the panel to either oscillate periodically about a buckled state or nonperiodically. The steady state response is dependent on the flow conditions and the initial deflection and velocity profiles of the panel. The flow Mach number and panel length-to-width ratios were varied. The cantilevered panel response is compared to previous research. A simply supported panel is briefly discussed and its response is also compared to previous work.

## **SECTION I**

### **Introduction**

This effort extends the research of Weiliang and Dowell, Reference 1, in which the response of a cantilevered panel was studied subject to supersonic flow over its upper surface. Weiliang and Dowell used Rayleigh-Ritz assumed modes to approximate the in-plane and transverse displacements. They performed a modal convergence study on the transverse displacements for several length-to-width ratio panels ranging from 0.25 to 10. A modal convergence study is included here on the in-plane and transverse displacements for two length-to-width ratio panels, 1 and 2.

Cantilevered panels are studied because their response can be used to estimate the response of the side of an aircraft inlet duct or the side of a flexible radome. With little modification, this analysis could estimate the response of low aspect ratio wings immersed in a supersonic flow.

Section II of this document discusses the analytical procedure used in determining the response of this thin, isotropic panel. The equations of motion stated in this Section were derived in Reference 2 for a panel with unspecified boundary conditions subject to multiple loading conditions. The modal functions used in the approximation of the displacements are stated as well. The procedure used to solve the resulting initial condition problem is discussed at the end of the Section.

The results of the analytical analyses performed in this effort are presented in Section III. The results include the modal convergence study and the response of the panel to various flow conditions. The response of the panel is shown using time histories, power spectral density, modified Poincaré, phase plane, and average time history plots. The flutter mode shape and modal contribution plots are shown also.

Finally, Section IV compares the current results to those in previous research studies. This comparison includes a panel with all edges simply supported subject to the above flow conditions. This panel is investigated to show that the technique is applicable to panels with other boundary conditions.



## SECTION II

### Analytical Procedure

The equations describing the motion of a thin panel subject to supersonic flow over the upper surface were derived in Reference 2. These equations were derived assuming the following: (1) the panel material is isotropic, (2) the panel deflections do not exceed the stress-strain proportional limits, (3) the stresses through the thickness are neglected because the panel thickness is much smaller than its length or width, (4) the panel is symmetric about its midplane, (5) the panel slope never exceeds about  $10^{-1}$ , and (6) the in-plane inertial terms are neglected because the in-plane displacements are small compared to the transverse displacements.

Nonlinear strain-displacement and linear stress-strain relations were used to determine the total strain energy in the panel. Rayleigh-Ritz approximate modes were introduced to define the nature of the panel deflection in each coordinate direction. The modal functions were not initially further specified so that the equations would apply to any rectangular panel that satisfied the previous assumptions. The energy expressions were nondimensionalized and substituted into a nondimensional form of Lagrange's equation from which the equations of motion were defined.

The nonconservative forces acting on the panel are due to the supersonic flow over the upper surface of the panel. A first order expansion in reduced frequency of the exact two dimensional, unsteady, linearized, potential flow equation predicts the unsteady aerodynamic forces on the panel. This theory is applicable over the Mach number range  $1.2 \leq M_\infty \leq 5.0$  and for low reduced frequencies. At high Mach number, this expression coincides with piston theory.

Considering these assumptions, the applicable equations of motion from Reference 2 are restated here.

#### U Equation

The nondimensional modal equation describing the deflections in the x direction is

$$\begin{aligned}
 & 2 \left\{ \int \frac{\partial \alpha_k}{\partial \bar{x}} \frac{\partial \alpha_i}{\partial \bar{x}} d\bar{x} \int \beta_l \beta_j d\bar{y} + \frac{(1-\nu)}{2} \left( \frac{a}{b} \right)^2 \int \alpha_k \alpha_i d\bar{x} \int \frac{\partial \beta_l}{\partial \bar{y}} \frac{\partial \beta_j}{\partial \bar{y}} d\bar{y} \right\} \bar{a}_{kl} \\
 & + 2 \frac{a}{b} \left\{ \nu \int \alpha_k \frac{\partial \alpha_i}{\partial \bar{x}} d\bar{x} \int \frac{\partial \beta_l}{\partial \bar{y}} \beta_j d\bar{y} + \frac{(1-\nu)}{2} \int \frac{\partial \alpha_k}{\partial \bar{x}} \alpha_i d\bar{x} \int \beta_l \frac{\partial \beta_j}{\partial \bar{y}} d\bar{y} \right\} \bar{b}_{kl} \\
 & = - \frac{h}{a} \left\{ \int \frac{\partial \phi_k}{\partial \bar{x}} \frac{\partial \phi_m}{\partial \bar{x}} \frac{\partial \alpha_i}{\partial \bar{x}} d\bar{x} \int \psi_l \psi_n \beta_j d\bar{y} \right. \\
 & \quad \left. + \nu \left( \frac{a}{b} \right)^2 \int \phi_k \phi_m \frac{\partial \alpha_i}{\partial \bar{x}} d\bar{x} \int \frac{\partial \psi_l}{\partial \bar{y}} \frac{\partial \psi_n}{\partial \bar{y}} \beta_j d\bar{y} \right\}
 \end{aligned}$$

$$+ (1-\nu) \left( \frac{a}{b} \right)^2 \int \phi_k \frac{\partial \phi_m}{\partial \bar{x}} \alpha_i d\bar{x} \int \frac{\partial \psi_l}{\partial \bar{y}} \psi_n \frac{\partial \beta_j}{\partial \bar{y}} d\bar{y} \left\} \bar{c}_{kl} \bar{c}_{mn} \quad (1)$$

v Equation

The nondimensional modal equation describing the deflections in the y direction is

$$\begin{aligned} & 2 \frac{a}{b} \left\{ \nu \int \frac{\partial \alpha_k}{\partial \bar{x}} \alpha_i d\bar{x} \int \beta_l \frac{\partial \beta_j}{\partial \bar{y}} d\bar{y} + \frac{(1-\nu)}{2} \int \alpha_k \frac{\partial \alpha_i}{\partial \bar{x}} d\bar{x} \int \frac{\partial \beta_l}{\partial \bar{y}} \beta_j d\bar{y} \right\} \bar{a}_{kl} \\ & + 2 \left\{ \left( \frac{a}{b} \right)^2 \int \alpha_k \alpha_i d\bar{x} \int \frac{\partial \beta_l}{\partial \bar{y}} \frac{\partial \beta_j}{\partial \bar{y}} d\bar{y} + \frac{(1-\nu)}{2} \int \frac{\partial \alpha_k}{\partial \bar{x}} \frac{\partial \alpha_i}{\partial \bar{x}} d\bar{x} \int \beta_l \beta_j d\bar{y} \right\} \bar{b}_{kl} \\ & = - \frac{h}{b} \left\{ \left( \frac{a}{b} \right)^2 \int \phi_k \phi_m \alpha_i d\bar{x} \int \frac{\partial \psi_l}{\partial \bar{y}} \frac{\partial \psi_n}{\partial \bar{y}} \frac{\partial \beta_j}{\partial \bar{y}} d\bar{y} \right. \\ & \quad + \nu \int \frac{\partial \phi_k}{\partial \bar{x}} \frac{\partial \phi_m}{\partial \bar{x}} \alpha_i d\bar{x} \int \psi_l \psi_n \frac{\partial \beta_j}{\partial \bar{y}} d\bar{y} \\ & \quad \left. + (1-\nu) \int \frac{\partial \phi_k}{\partial \bar{x}} \phi_m \frac{\partial \alpha_i}{\partial \bar{x}} d\bar{x} \int \psi_l \frac{\partial \psi_n}{\partial \bar{y}} \beta_j d\bar{y} \right\} \bar{c}_{kl} \bar{c}_{mn} \quad (2) \end{aligned}$$

w Equation

The nondimensional modal equation describing the transverse deflections is

$$\begin{aligned} & \frac{1}{6} \left\{ \int \phi_k \phi_l d\bar{x} \int \psi_i \psi_j d\bar{y} \right\} \ddot{\bar{c}}_{kl} \\ & + \frac{1}{6} \left\{ \int \frac{\partial^2 \phi_k}{\partial \bar{x}^2} \frac{\partial^2 \phi_l}{\partial \bar{x}^2} d\bar{x} \int \psi_i \psi_j d\bar{y} + \left( \frac{a}{b} \right)^4 \int \phi_k \phi_l d\bar{x} \int \frac{\partial^2 \psi_i}{\partial \bar{y}^2} \frac{\partial^2 \psi_j}{\partial \bar{y}^2} d\bar{y} \right. \\ & \quad + \nu \left( \frac{a}{b} \right)^2 \left[ \int \frac{\partial^2 \phi_k}{\partial \bar{x}^2} \phi_l d\bar{x} \int \psi_i \frac{\partial^2 \psi_j}{\partial \bar{y}^2} d\bar{y} + \int \phi_k \frac{\partial^2 \phi_l}{\partial \bar{x}^2} d\bar{x} \int \frac{\partial^2 \psi_i}{\partial \bar{y}^2} \psi_j d\bar{y} \right] \\ & \quad \left. + 2(1-\nu) \left( \frac{a}{b} \right)^2 \int \frac{\partial \phi_k}{\partial \bar{x}} \frac{\partial \phi_l}{\partial \bar{x}} d\bar{x} \int \frac{\partial \psi_i}{\partial \bar{y}} \frac{\partial \psi_j}{\partial \bar{y}} d\bar{y} \right\} \bar{c}_{kl} \\ & + \left\{ \int \frac{\partial \phi_k}{\partial \bar{x}} \frac{\partial \phi_m}{\partial \bar{x}} \frac{\partial \phi_o}{\partial \bar{x}} \frac{\partial \phi_i}{\partial \bar{x}} d\bar{x} \int \psi_l \psi_n \psi_p \psi_j d\bar{y} + \left( \frac{a}{b} \right)^4 \int \phi_k \phi_m \phi_o \phi_i d\bar{x} \int \frac{\partial \psi_l}{\partial \bar{y}} \frac{\partial \psi_n}{\partial \bar{y}} \frac{\partial \psi_p}{\partial \bar{y}} \frac{\partial \psi_j}{\partial \bar{y}} d\bar{y} \right. \\ & \quad + \left( \frac{a}{b} \right)^2 \int \phi_k \frac{\partial \phi_m}{\partial \bar{x}} \frac{\partial \phi_o}{\partial \bar{x}} \phi_i d\bar{x} \int \frac{\partial \psi_l}{\partial \bar{y}} \psi_n \psi_p \frac{\partial \psi_j}{\partial \bar{y}} d\bar{y} \\ & \quad \left. + \left( \frac{a}{b} \right)^2 \int \frac{\partial \phi_k}{\partial \bar{x}} \phi_m \phi_o \frac{\partial \phi_i}{\partial \bar{x}} d\bar{x} \int \psi_l \frac{\partial \psi_n}{\partial \bar{y}} \frac{\partial \psi_p}{\partial \bar{y}} \psi_j d\bar{y} \right\} \bar{c}_{kl} \bar{c}_{mn} \bar{c}_{op} \end{aligned}$$

$$\begin{aligned}
& + 2 \frac{a}{h} \left\{ \int \frac{\partial \alpha_k}{\partial \bar{x}} \frac{\partial \phi_m}{\partial \bar{x}} \frac{\partial \phi_i}{\partial \bar{x}} d\bar{x} \int \beta_l \psi_n \psi_j d\bar{y} + v \left( \frac{a}{b} \right)^2 \int \frac{\partial \alpha_k}{\partial \bar{x}} \phi_m \phi_i d\bar{x} \int \beta_l \frac{\partial \psi_n}{\partial \bar{y}} \frac{\partial \psi_j}{\partial \bar{y}} d\bar{y} \right. \\
& \quad + \frac{(1-v)}{2} \left( \frac{a}{b} \right)^2 \int \alpha_k \phi_m \frac{\partial \phi_i}{\partial \bar{x}} d\bar{x} \int \frac{\partial \beta_l}{\partial \bar{y}} \frac{\partial \psi_n}{\partial \bar{y}} \psi_j d\bar{y} \\
& \quad \left. + \frac{(1-v)}{2} \left( \frac{a}{b} \right)^2 \int \alpha_k \frac{\partial \phi_m}{\partial \bar{x}} \phi_i d\bar{x} \int \frac{\partial \beta_l}{\partial \bar{y}} \psi_n \frac{\partial \psi_j}{\partial \bar{y}} d\bar{y} \right\} \bar{c}_{mn} \bar{a}_{kl} \\
& + 2 \frac{a}{b} \frac{a}{h} \left\{ \left( \frac{a}{b} \right)^2 \int \alpha_k \phi_m \phi_i d\bar{x} \int \frac{\partial \beta_l}{\partial \bar{y}} \frac{\partial \psi_n}{\partial \bar{y}} \frac{\partial \psi_j}{\partial \bar{y}} d\bar{y} + v \int \alpha_k \frac{\partial \phi_m}{\partial \bar{x}} \frac{\partial \phi_i}{\partial \bar{x}} d\bar{x} \int \frac{\partial \beta_l}{\partial \bar{y}} \psi_n \psi_j d\bar{y} \right. \\
& \quad + \frac{(1-v)}{2} \int \frac{\partial \alpha_k}{\partial \bar{x}} \phi_m \frac{\partial \phi_i}{\partial \bar{x}} d\bar{x} \int \beta_l \frac{\partial \psi_n}{\partial \bar{y}} \psi_j d\bar{y} \\
& \quad \left. + \frac{(1-v)}{2} \int \frac{\partial \alpha_k}{\partial \bar{x}} \frac{\partial \phi_m}{\partial \bar{x}} \phi_i d\bar{x} \int \beta_l \psi_n \frac{\partial \psi_j}{\partial \bar{y}} d\bar{y} \right\} \bar{c}_{mn} \bar{b}_{kl} \\
& = - \frac{\lambda}{6\beta} \left\{ \left[ \int \frac{\partial \phi_k}{\partial \bar{x}} \phi_i d\bar{x} \int \psi_l \psi_j d\bar{y} \right] \bar{c}_{kl} + \left( \frac{M^2 - 2}{M^2 - 1} \right) \left( \frac{\mu}{\lambda} \right)^{\frac{1}{2}} \left[ \int \phi_k \phi_i d\bar{x} \int \psi_l \psi_j d\bar{y} \right] \dot{\bar{c}}_{kl} \right\} \quad (3)
\end{aligned}$$

where the indices on  $\alpha$  range between one and the total number of in-plane modes in the  $x$  direction, on  $\beta$  between one and the total number of in-plane modes in the  $y$  direction, on  $\phi$  between one and the total number of transverse modes in the  $x$  direction, and on  $\psi$  between one and the total number of transverse modes in the  $y$  direction.

Equations (1)-(3) are applicable to any panel that meets the assumptions stated at the beginning of this section. Each deflection is approximated using the product of a time varying weighting function and two modal functions.

$$\bar{u}(\bar{x}, \bar{y}, \tau) = \bar{a}_{ij}(\tau) \alpha_i(\bar{x}) \beta_j(\bar{y}) \quad \text{where } 1 \leq i \leq NXU \text{ and } 1 \leq j \leq NYU \quad (4a)$$

$$\bar{v}(\bar{x}, \bar{y}, \tau) = \bar{b}_{kl}(\tau) \alpha_k(\bar{x}) \beta_l(\bar{y}) \quad \text{where } 1 \leq k \leq NXV \text{ and } 1 \leq l \leq NYV \quad (4b)$$

$$\bar{w}(\bar{x}, \bar{y}, \tau) = \bar{c}_{mn}(\tau) \phi_m(\bar{x}) \psi_n(\bar{y}) \quad \text{where } 1 \leq m \leq NXW \text{ and } 1 \leq n \leq NYW \quad (4c)$$

The modal functions satisfy the panel boundary conditions only and are called Rayleigh-Ritz modal functions. The convention of summing over repeated indices is used.

The Rayleigh-Ritz modal functions must be defined for the specific panel under investigation. In the present case, the panel is fixed along the  $y = 0$  axis and free on all other sides (Figure 1). One of the modal functions used to represent each deflection approximates the deflection of a beam that is fixed at one end and free at the other. The other modal function approximates the deflection of a beam that is free at both ends. The modal functions that define the in-plane deflections are

$$\alpha_i(\bar{x}) = \cos(i\pi\bar{x}) \quad (5)$$

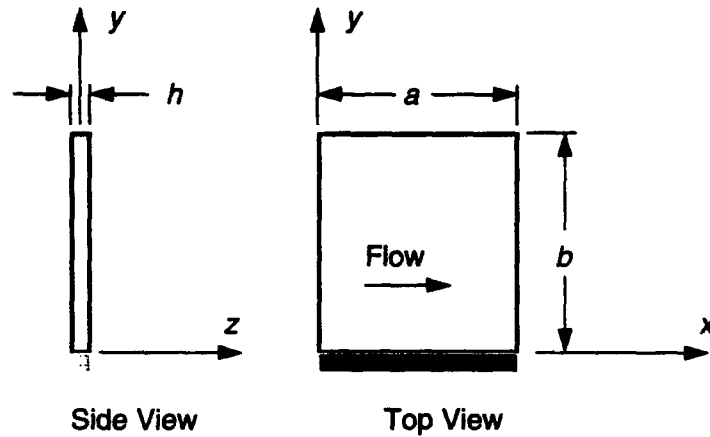


Figure 1 Side and top views of panel under investigation.

$$\beta_j(\bar{y}) = \sin[(j-0.50)\pi\bar{y}] \quad (6)$$

and the modal functions that define the transverse deflection are

$$\phi_i(\bar{x}) = \begin{cases} 2 & \text{for } i = 1 \\ 2(1-2\bar{x}) & \text{for } i = 2 \\ \sqrt{2}\sin[(i-1.50)\pi\bar{x} + 0.75\pi] + e^{-(i-1.50)\pi\bar{x}} - (-1)^{i-2}e^{-(i-1.50)\pi(1-\bar{x})} & \text{for } i > 2 \end{cases} \quad (7)$$

$$\psi_j(\bar{y}) = \sqrt{2}\sin[(j-0.50)\pi\bar{y} - 0.25\pi] + e^{-(j-0.50)\pi\bar{y}} - (-1)^j e^{-(j-0.50)\pi(1-\bar{y})} + (-1)^j e^{-(j-0.50)\pi} \quad (8)$$

The first two  $\phi$  modes represent the rigid translation and rotation modes of a free-free beam, respectively. Expressions (5)-(8) are the same modal functions that were employed in the nonlinear panel flutter investigation in Reference 1 and are derived in References 3 and 4.

The solutions to Equations (1)-(3) are three time dependent functions that describe the motion of a cantilevered panel as prescribed by Equations (5)-(8). The closed-form analytical solutions of these equations, if they exist, are not determined here. However, these equations are solved numerically. Equations (5)-(8) are substituted into Equations (1)-(3) and the spatial integrations are performed using an extended Simpson's rule (Reference 5):

$$\int_{x_1}^{x_N} f(x) dx = h \left[ \frac{1}{3}f_1 + \frac{4}{3}f_2 + \frac{2}{3}f_3 + \frac{4}{3}f_4 + \dots + \frac{2}{3}f_{N-2} + \frac{4}{3}f_{N-1} + \frac{1}{3}f_N \right] + O\left(\frac{1}{N^4}\right) \quad (9)$$

Equation (3) is rewritten in state-space form once the spatial integrations are performed and the following procedure is used to solve the remaining initial condition problem.

- 1)  $\bar{c}(\tau=0)$  and  $\dot{\bar{c}}(\tau=0)$  are assumed.

- 2)  $\bar{a}$  and  $\bar{b}$  are determined by solving Equations (1) and (2) simultaneously.
- 3)  $\bar{c}(\tau + \Delta\tau)$  is determined by integrating the state-space form of Equation (3).
- 4) Return to step 2 until a steady state response is reached.

The initial conditions used throughout all the analyses are

$$\bar{c}(\tau=0) = \begin{cases} \bar{c}_{11} = 0.001/h \\ \bar{c}_{mn} = 0.000 \end{cases} \text{ for all } m \text{ and } n \text{ except } m = n = 1 \quad (10)$$

$$\dot{\bar{c}}(\tau=0) = 0$$

unless otherwise specified and the integration in step 3 is performed using a Kutta-Simpson one-third rule as outlined in Reference 6.

## SECTION III

### Numerical Results

As mentioned in the last section, Equations (1)-(3) were solved numerically. A computer program was written and run on a CONVEX mainframe and SUN Iris workstation. The program was vector optimized on both machines for fast operation. It was written such that the spatial integrations were performed once for the specified number of in-plane and transverse modal functions, or more specifically structural modes, and written to a file. This operation was performed so that the spatial integrations could be read instead of recomputed each time the flow conditions were changed. Therefore, the code ran faster for each new flow case. An interactive plotting routine was incorporated to provide viewing and documenting results.

This section documents the results of a numerical study of a cantilevered panel. Before examining the flutter response of the panel, the number of structural modes required to predict accurate results within the given assumptions needs to be determined. A detailed investigation of the panel response versus number of modes and flow conditions follows. Two panel length-to-width ratios ( $a/b$ ) and three freestream Mach numbers are examined. The initial conditions are varied to determine their effect on the steady state response of the panel.

The following parameters are used in all cases unless otherwise stated:  $a = 1\text{ m}$ ,  $h = 0.01\text{ m}$ ,  $\nu = 0.33$ ,  $\mu = 0.10$ ,  $E = 7.10 \times 10^{10}\text{ N/m}^2$ , and  $\alpha = 2.33 \times 10^{-5}\text{ }^\circ\text{C}$ . The data on the right side of each figure define the specific panel parameters and flow conditions for which the curves were generated. Throughout this effort, the number of modal functions used in the  $x$  direction to approximate  $u$  is the same number used in approximating  $v$  ( $NXU = NXV$ ). Similarly, the number of modal functions used in the  $y$  direction to approximate both in-plane displacements is the same ( $NYU = NYV$ ). The responses shown in the figures reflect the panel response at location  $x = 0.75a$  and  $y = b$ .

#### Modal Convergence

The convergence study was iterative in nature. The number of transverse modes was varied using one in-plane mode in each direction. Then the number of in-plane modes was varied using the converged transverse results. Finally, the number of transverse modes was varied again to confirm the previous transverse results but with the converged in-plane results. The results of this study follow.

$a/b = 1$

Figure 2 compares the response of a panel when different numbers of transverse modes in the  $x$  direction and  $NYW=2$  are used. Note that the difference between the  $NXW=6$  and the  $NXW=8$  curves is smaller than the difference between the  $NXW=4$  and  $NXW=6$  curves. If one wanted the least number of modes that gives the closest results to that of an analysis using a large number of modes, one would choose  $NXW=6$  to analyze  $a/b = 1$  panels. (The computation time is minimized when the fewest number of modes is incorporated.)

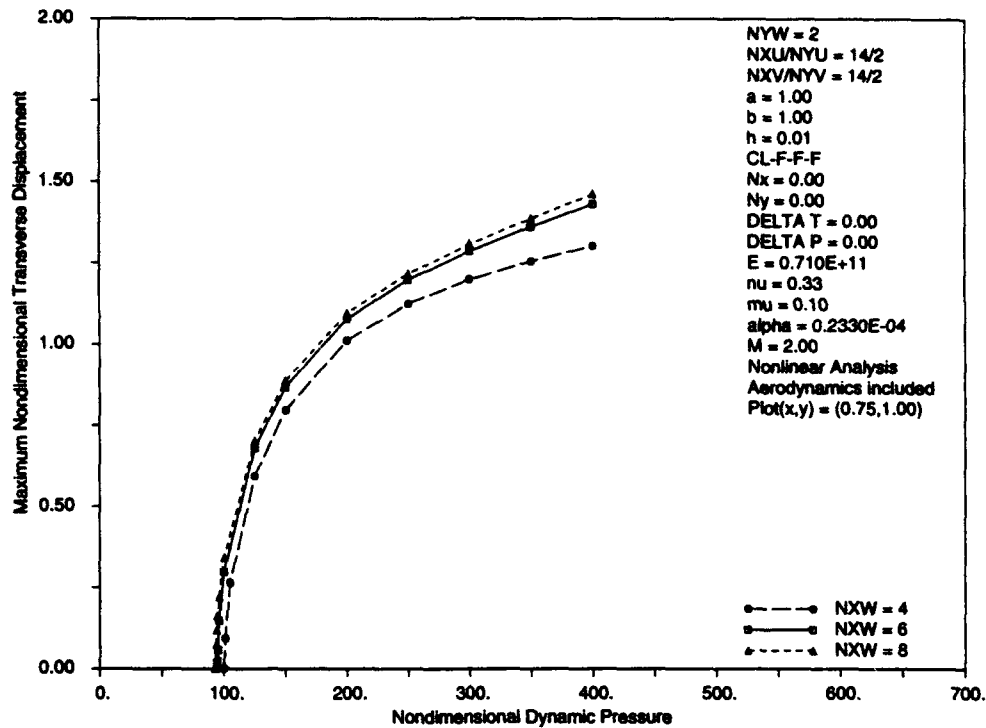


Figure 2 Transverse mode number variation in x direction ( $a/b = 1$ ).

Figure 3 is a plot comparing the panel response to different NYW for the same in-plane modal combination as in Figure 2 and  $NXW=6$ . Note that the  $NYW=2$  curve has the same basic character and is closest to the  $NYW=3$  curve. Therefore,  $NYW=2$  was chosen for the subsequent analyses of  $a/b = 1$  panels.

Figure 4 is a plot comparing the panel response to different numbers of in-plane modes used to define the deflection in the x direction. In this figure  $NYU=NYV=1$  was used. The transverse displacement amplitude increases as the in-plane modal number increases for a given nondimensional dynamic pressure. The  $NXU=NXV=13$  through 16 curves are much closer to each other than any of the other curves.  $NXU=NXV=14$  was chosen for the subsequent analyses.

The inverse number of in-plane modes in the x direction is plotted against the maximum nondimensional steady state transverse displacement normalized using the  $NXU=NXV=16$  value for  $\lambda=300$  in Figure 5. The normalized displacement when an infinite number of in-plane modal functions in the x direction are included in the analysis can be extrapolated from this figure, approximately 1.05. It further shows that the normalized  $NXU=NXV=14$  result is within 5% of using  $NXU=NXV=\infty$ .

Finally, a plot comparing the  $a/b = 1$  panel response to different numbers of in-plane modes used in the y direction is shown in Figure 6. The transverse modal combination used here was  $NXW/NYW=6/2$ . Note that the two and three mode curves are almost identical and that the one

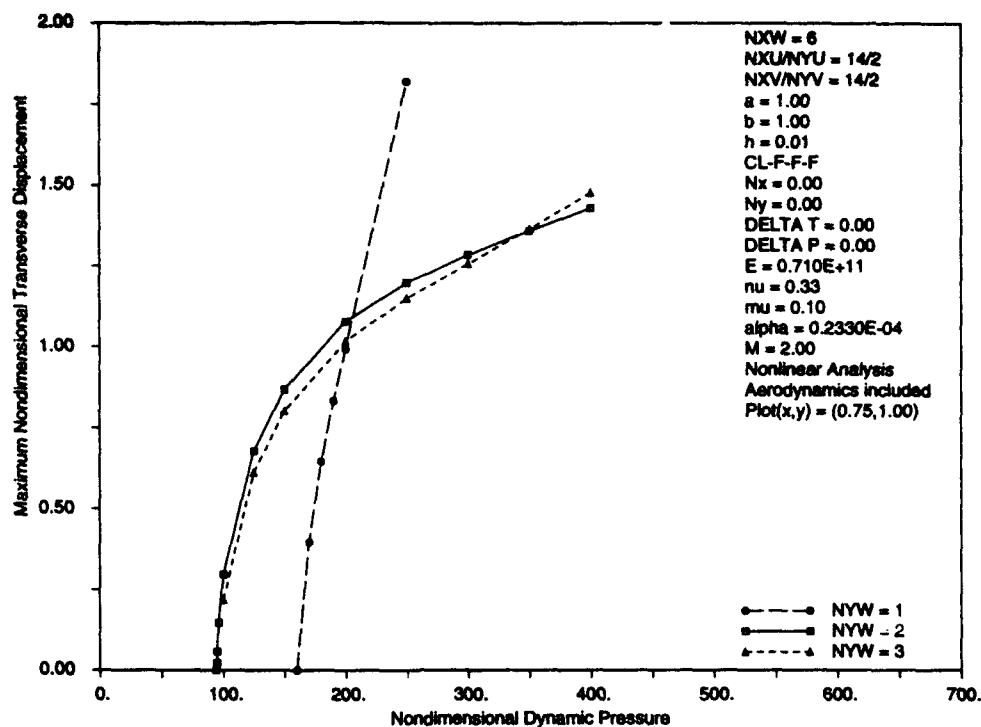


Figure 3 Transverse mode number variation in y direction ( $a/b = 1$ ).

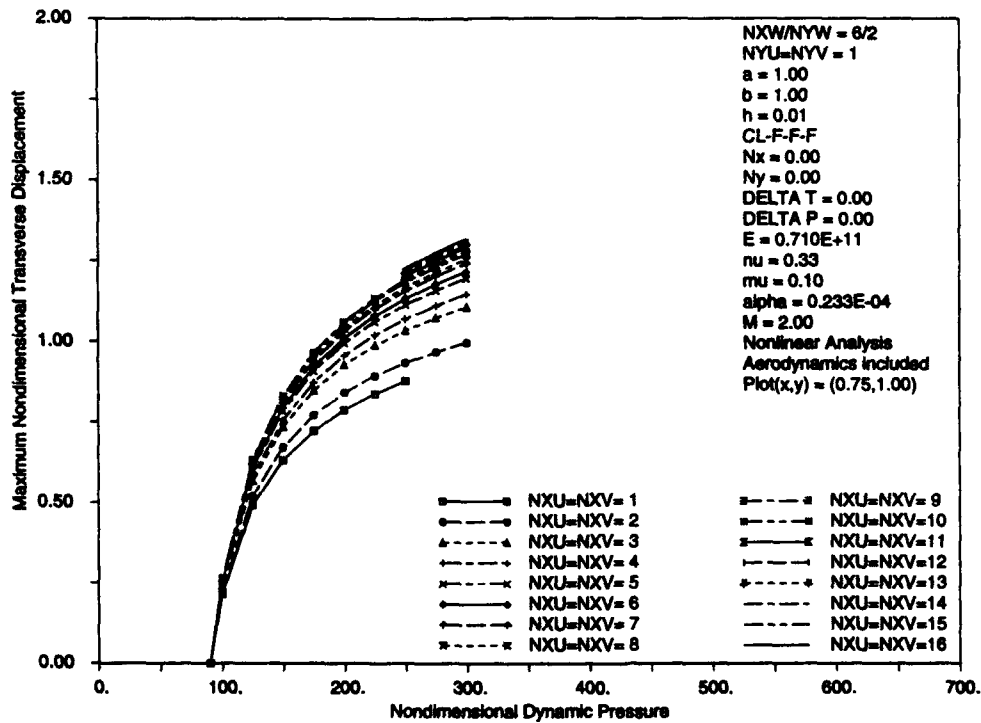


Figure 4 In-plane mode number variation in x direction ( $a/b = 1$ ).



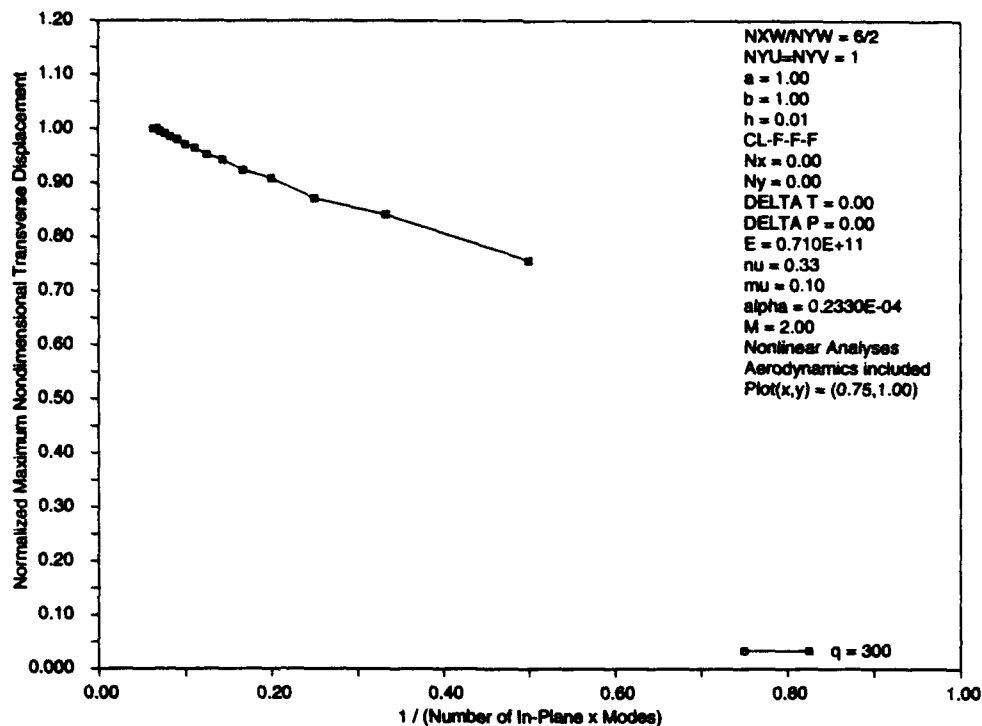


Figure 5 Reciprocal number of in-plane modes versus normalized maximum nondimensional transverse displacement.

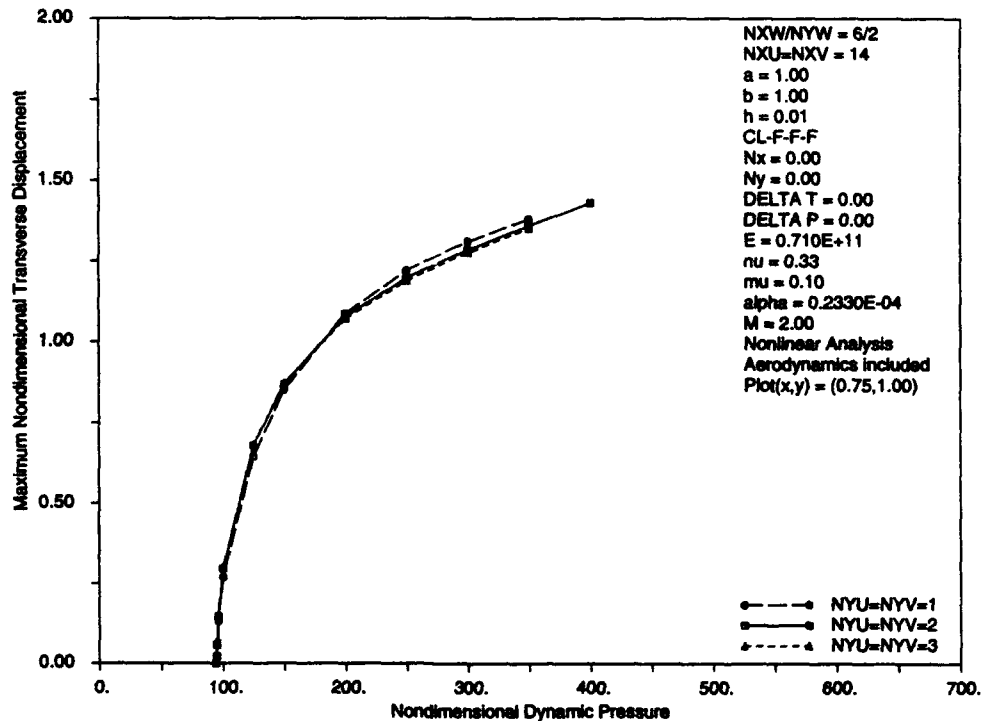


Figure 6 In-plane mode number variation in y direction ( $a/b = 1$ ).

mode curve is slightly different from the other two curves at higher nondimensional dynamic pressures. One could conclude from this figure that any one of these modal number options could be used. Two in-plane modes in the  $y$  direction were selected because it was determined that the increase in computation time over the one in-plane mode was minimal compared to the possible increase in displacement detail.

Figure 7 shows the maximum nondimensional steady state transverse response versus the nondimensional dynamic pressure divided by the compressibility factor,  $\beta$ , for three Mach numbers. Note that all three curves are coincident. Therefore, this figure shows that the steady state scaled response of an  $a/b = 1$  cantilevered panel with supersonic flow over its upper surface is essentially Mach number independent.

$a/b = 2$

Figure 8 compares the response of an  $a/b = 2$  panel to different NXW when NYW=2. The NXW=4 case was not included because it failed to produce a response curve like the ones in Figure 8 and its oscillation frequency was much higher than that associated with the other curves. The number of transverse modes in the  $x$  direction was selected to be 8 because the difference between the NXW=8 and NXW=10 curves was approximately one third of the difference between the NXW=6 and NXW=8 curves for large nondimensional dynamic pressures.

Figure 9 shows a comparison between different NXU=NXV curves. There is a small increase in nondimensional transverse displacement as the number of modes increases for a

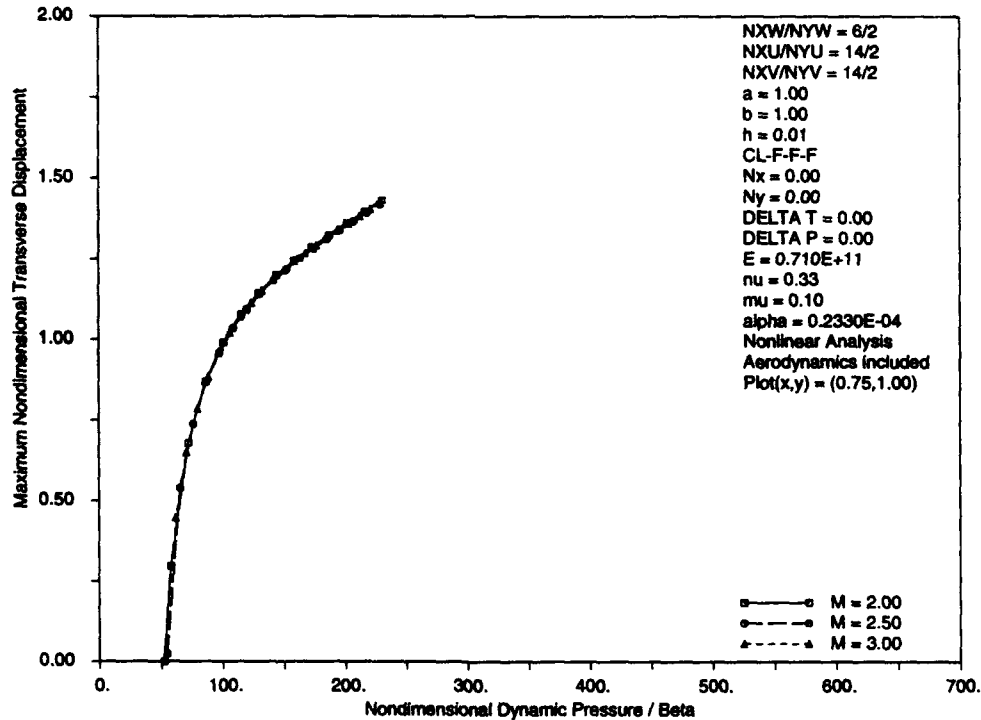


Figure 7 Mach number variation ( $a/b = 1$ ).

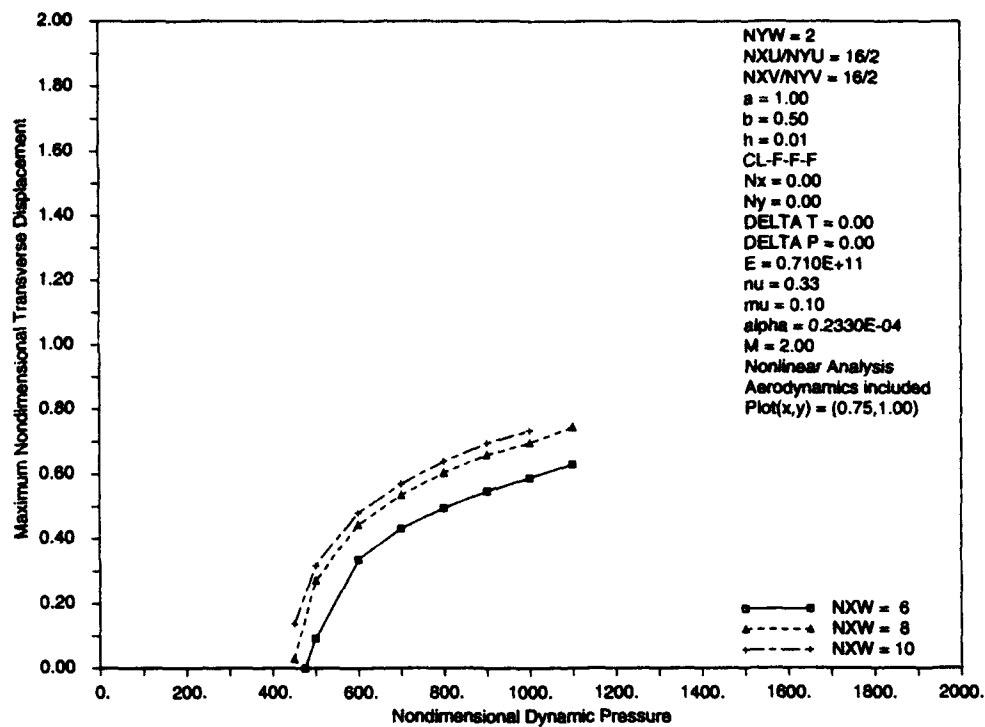


Figure 8 Transverse mode number variation in  $x$  direction ( $a/b = 2$ ).

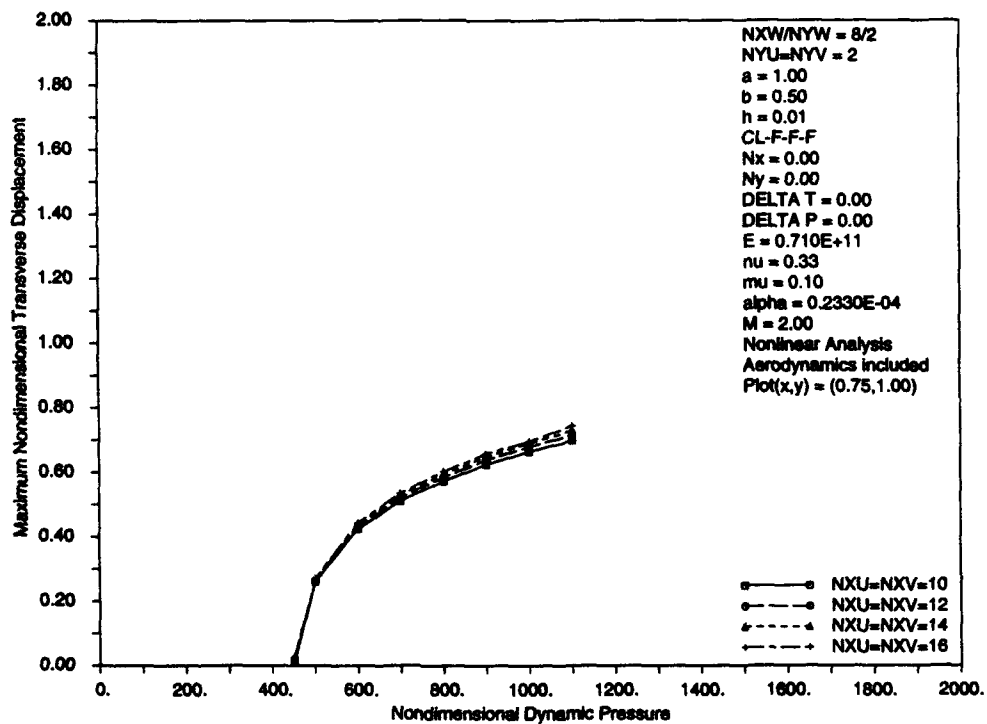


Figure 9 In-plane mode number variation in  $x$  direction ( $a/b = 2$ ).

specific nondimensional dynamic pressure. The number of in-plane modes in the  $x$  direction to be used in subsequent analyses was chosen to be 16.

The maximum nondimensional transverse displacement plotted against nondimensional dynamic pressure divided by the compressibility factor is shown in Figure 10 for three Mach numbers. Note that the scaled  $a/b = 2$  panel response is essentially independent of Mach number as well since the curves are coincident.

Figure 11 compares the converged maximum nondimensional transverse response of the  $a/b = 1$  and 2 panels. The nondimensional dynamic pressure at which the steady state response is no longer zero is the nondimensional flutter dynamic pressure,  $\lambda_F$ , or the condition at which the panel begins to flutter. Note that the  $a/b = 2$  panel has a higher  $\lambda_F$  than the  $a/b = 1$  panel. Also note that the rate at which the response increases with increasing  $\lambda$  for the  $a/b = 2$  panel is much slower than the  $a/b = 1$  panel.

The nondimensional time step used throughout this study was 0.005. Figure 12 is a plot comparing the maximum nondimensional transverse displacement for three different time steps at three different nondimensional dynamic pressures for the  $a/b = 1$  panel. The curves shown in this figure are nearly horizontal. The variation in displacement from one end of each curve to the other is less than 1 percent of the average displacement along each curve.

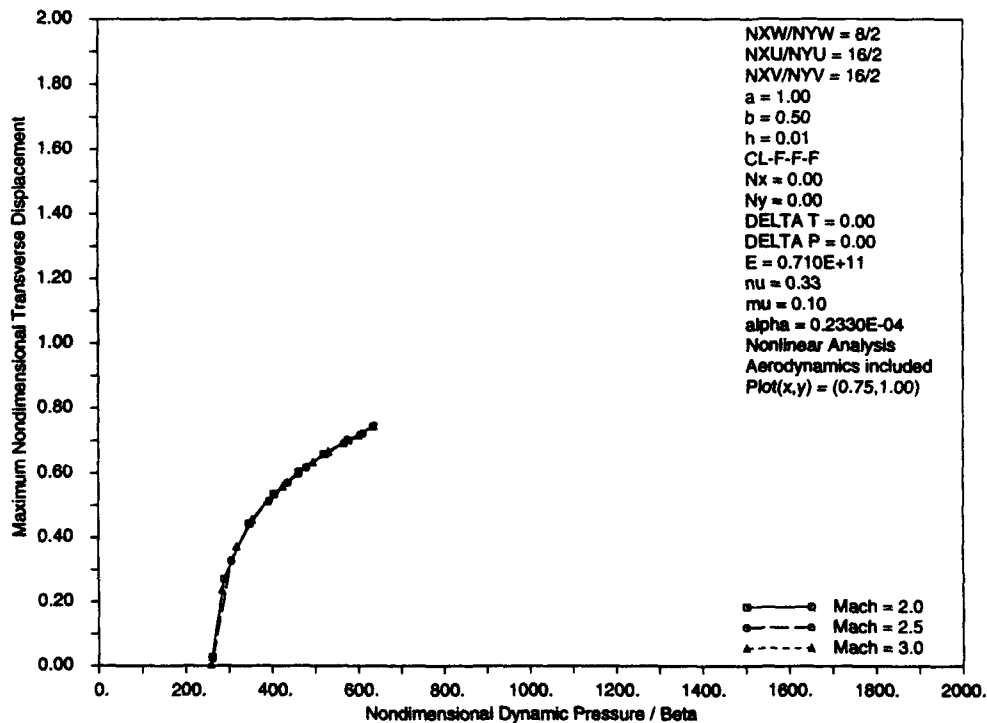


Figure 10 Mach number variation ( $a/b = 2$ ).

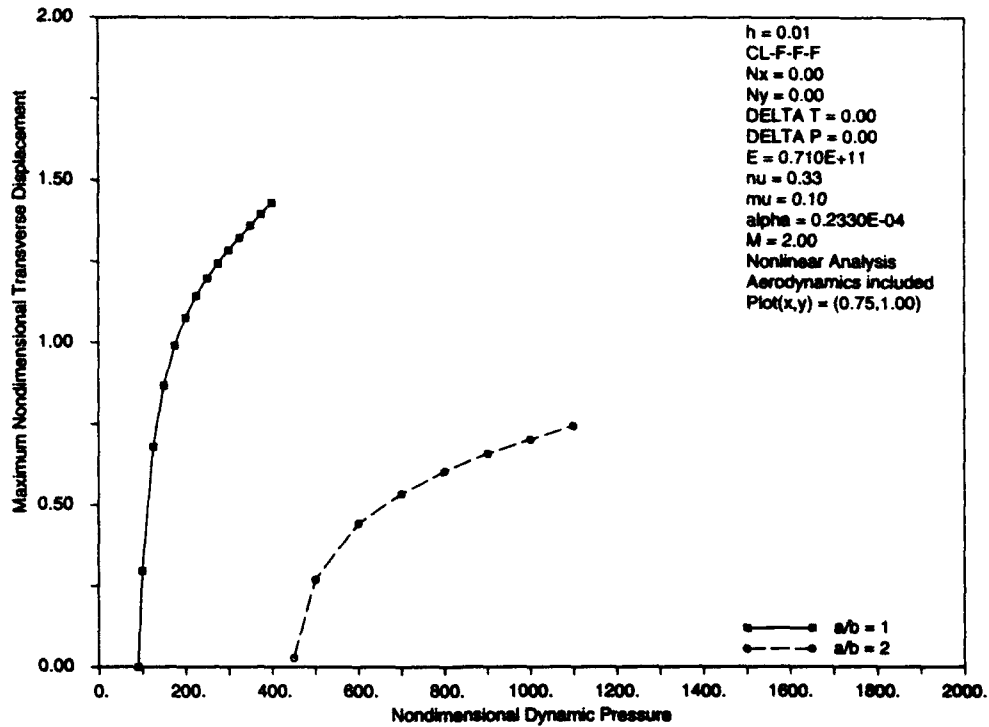


Figure 11 Plot comparing converged steady state response of  $a/b = 1$  and  $a/b = 2$  panels.

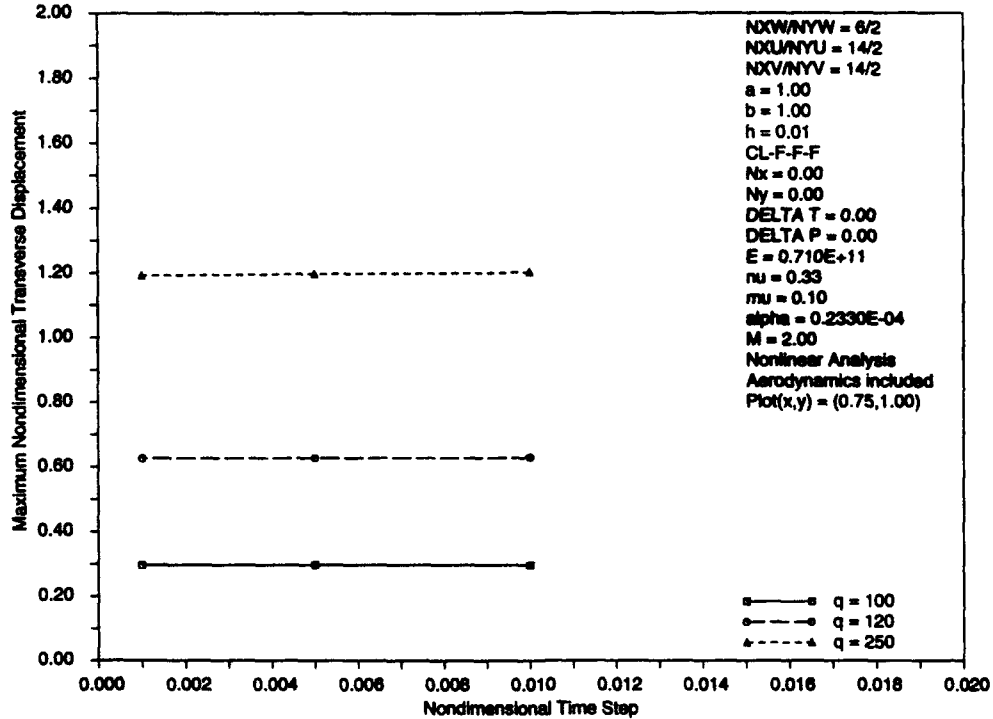


Figure 12 Maximum nondimensional transverse displacement variation with time step ( $a/b = 1$ ).

The transverse oscillation frequency varies as the nondimensional dynamic pressure and transverse displacement increase. Figure 13 shows the variation in frequency with nondimensional dynamic pressure along the converged  $a/b = 1$  panel curve shown in Figure 11. Note that the slope of this curve decreases as the dynamic pressure increases.

### Structural Response

The structural response of the panel was monitored by examining the time history, power spectral density (PSD), Poincaré, phase plane, the oscillation center, and modal contribution plots at location  $x = 0.75a$  and  $y = b$  and the flutter mode shape of the entire panel. When the flow conditions over the panel are lower than that required for flutter onset, the initial applied transverse deformations decay to zero as shown in Figure 14. The panel reaches a constant amplitude steady state oscillation when the flutter onset conditions have been exceeded and once the transients have decayed. Figures 15-21 show an example of the panel oscillating at approximately 1.27 times the flutter onset conditions. They include the in-plane and transverse time histories, the three dimensional flutter mode shape, the PSD, the modified Poincaré, the phase plane, the average transverse time history peak, and the transverse chordwise and spanwise modal contribution plots respectively.

Close examination of the in-plane and transverse displacements in Figures 15a-c reveals that as the panel deflects in both the positive and negative  $z$  directions, the in-plane displacement amplitudes increase in the negative  $x$  and  $y$  directions. Thus, the maximum transverse displacements, both positive and negative, correspond to the maximum negative in-plane

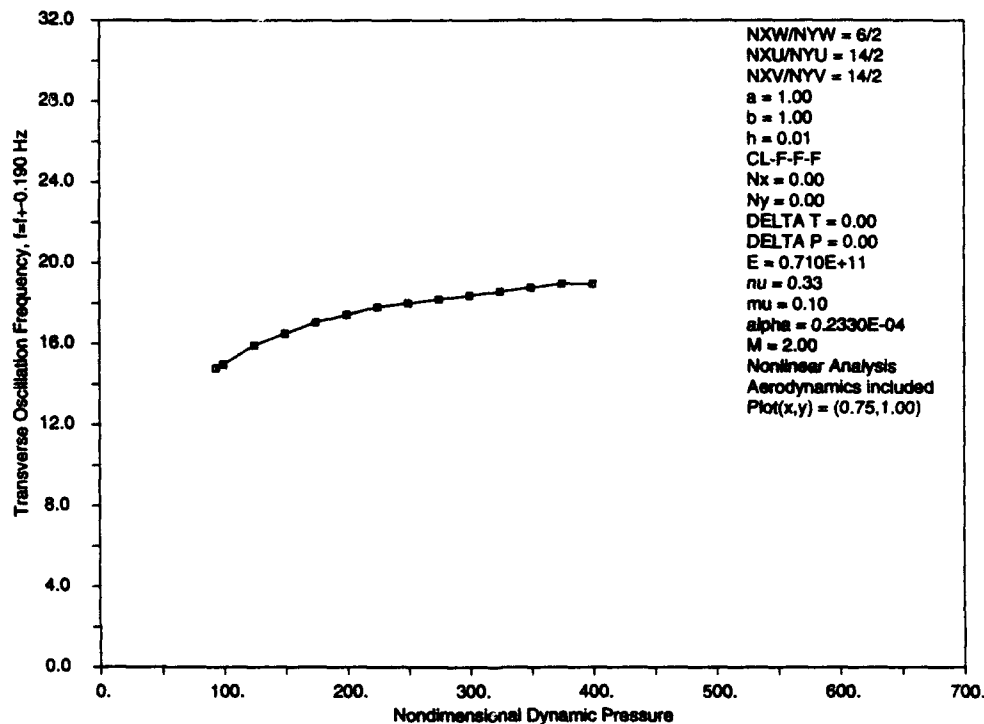


Figure 13 Transverse oscillation frequency variation along converged  $a/b = 1$  curve.

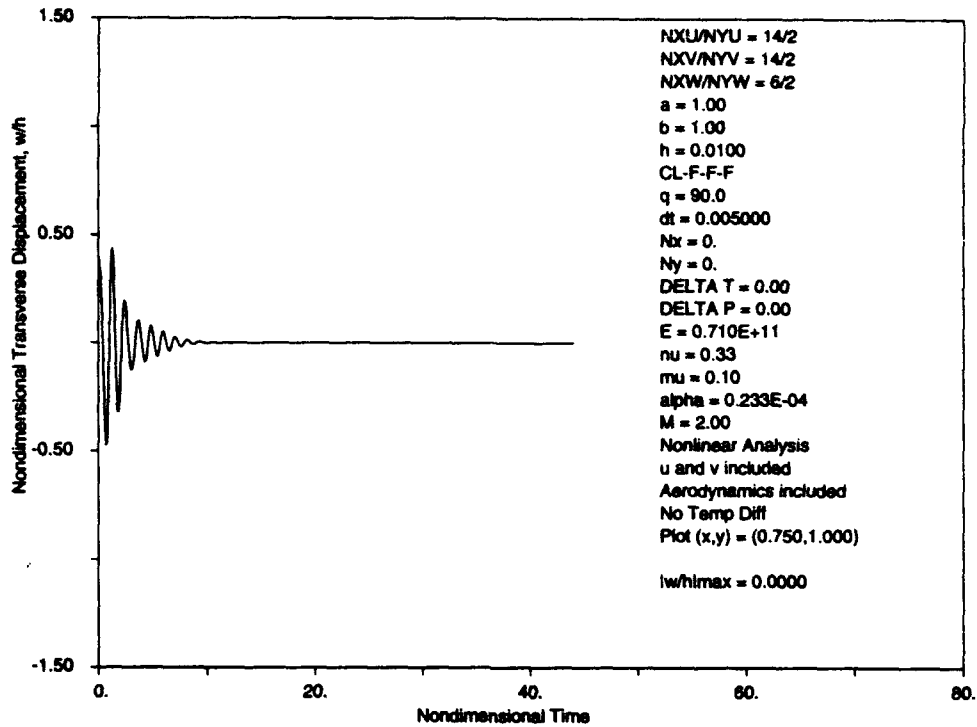


Figure 14 Transverse time history of location (0.75,1.00) where  $\lambda=90$  and  $a/b = 1$ .

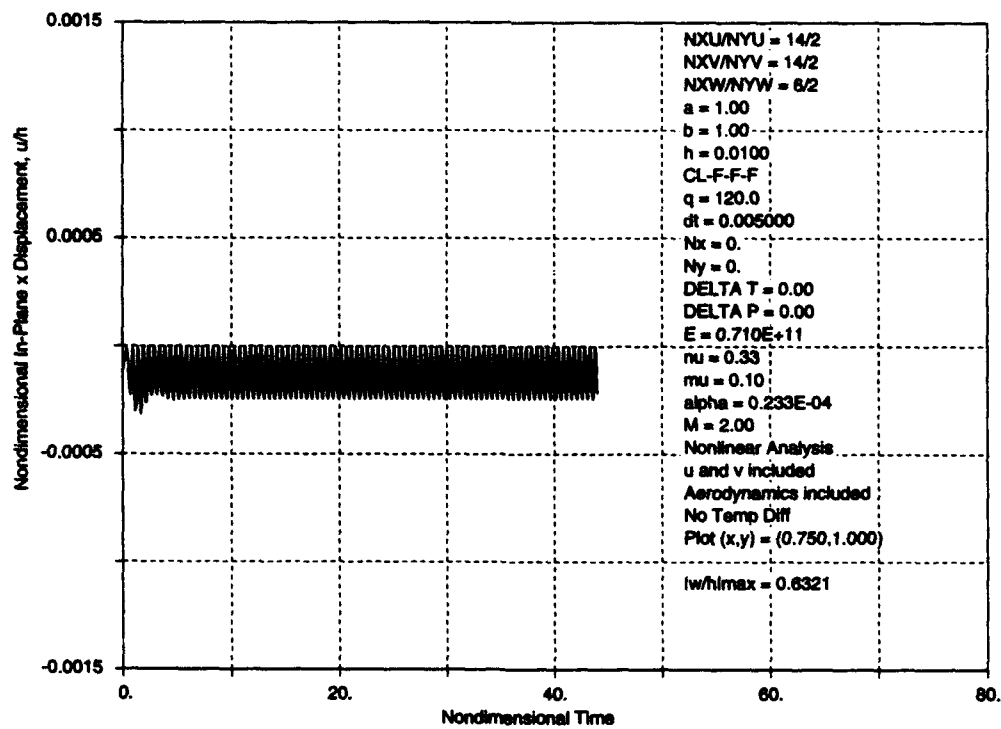


Figure 15a In-plane time history in the x direction of point (0.75,1.00) where  $\lambda=120$  and  $a/b = 1$ .

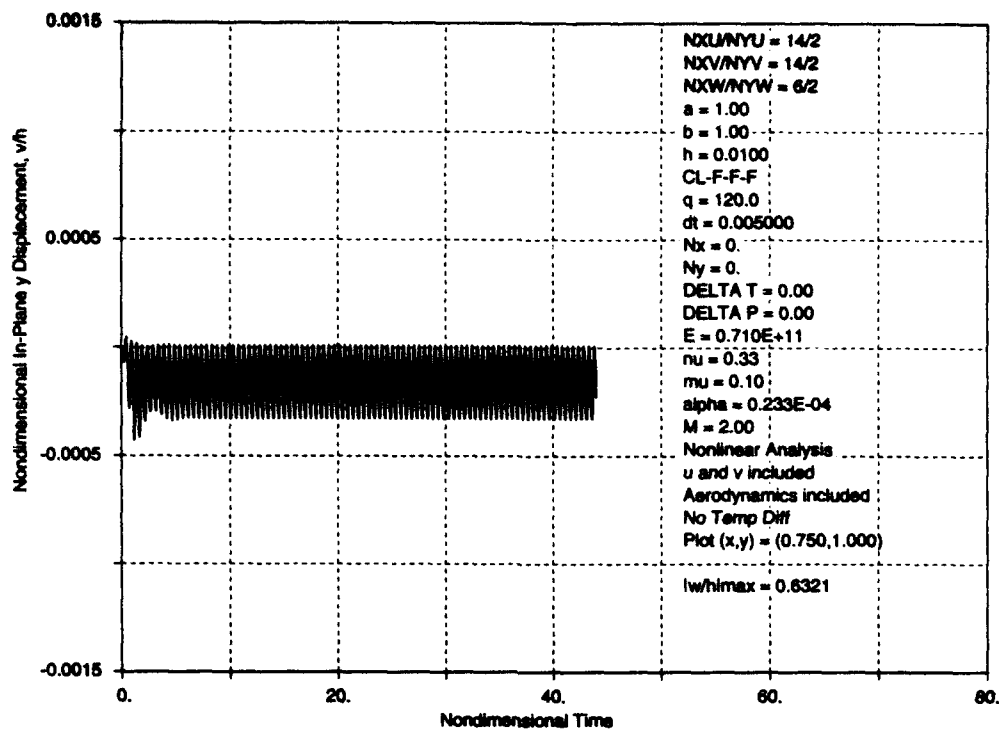


Figure 15b In-plane time history in the y direction of point (0.75,1.00) where  $\lambda=120$  and  $a/b = 1$ .

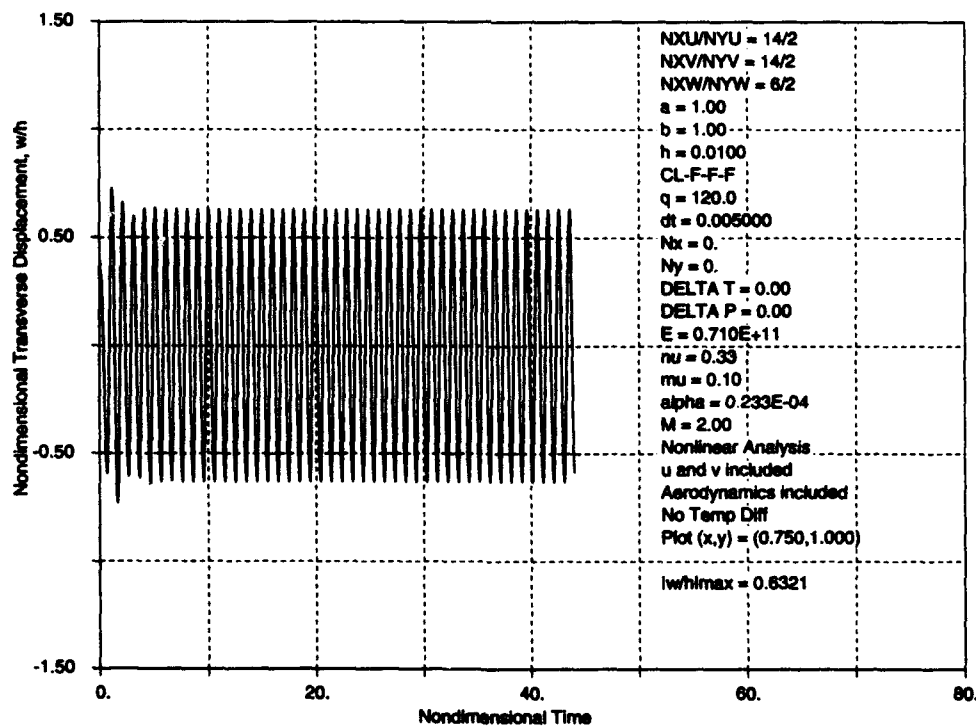


Figure 15c Transverse time history of location (0.75,1.00) where  $\lambda=120$  and  $a/b = 1$ .



displacements and the in-plane displacements oscillate at twice the transverse oscillation frequency. Note that the in-plane displacement in the  $x$  direction oscillates such that the displacement is never positive once the steady state is reached. The point at which the in-plane  $x$  displacement is at its smallest amplitude coincides with the point at which the transverse displacement is at its smallest amplitude. Note in Figure 15b that the in-plane displacement in the  $y$  direction has both positive and negative values. The in-plane  $y$  displacement is positive when the transverse displacement is at its smallest amplitude. Therefore, the panel is stretching in the  $y$  direction as it oscillates. Further note that the transverse displacement in Figure 15c oscillates about  $z = 0$  (Figure 20 confirms this visual inspection). The plot in Figure 15d displays the transverse displacement for the same analysis parameters in Figure 15c except the panel is restricted from moving in the  $x$  and  $y$  directions. Here, the transverse displacement is smaller and the transverse oscillation frequency is slightly lower: 15.4 Hz for the restricted case as compared to 15.7 Hz for the unrestricted case (see Figure 17).

Figure 16 shows the deflected panel at one of the later maximum transverse peaks in Figure 15c. The entire outboard edge is deflected with the trailing edge deflected more than any other point. The slope of the outboard edge is nearly constant.

The power spectral density plot derived from the response of the outboard three-quarter chord point is shown in Figure 17. This figure shows that the panel is oscillating at essentially one frequency for the given flow conditions. The first ten nondimensional transverse oscillation

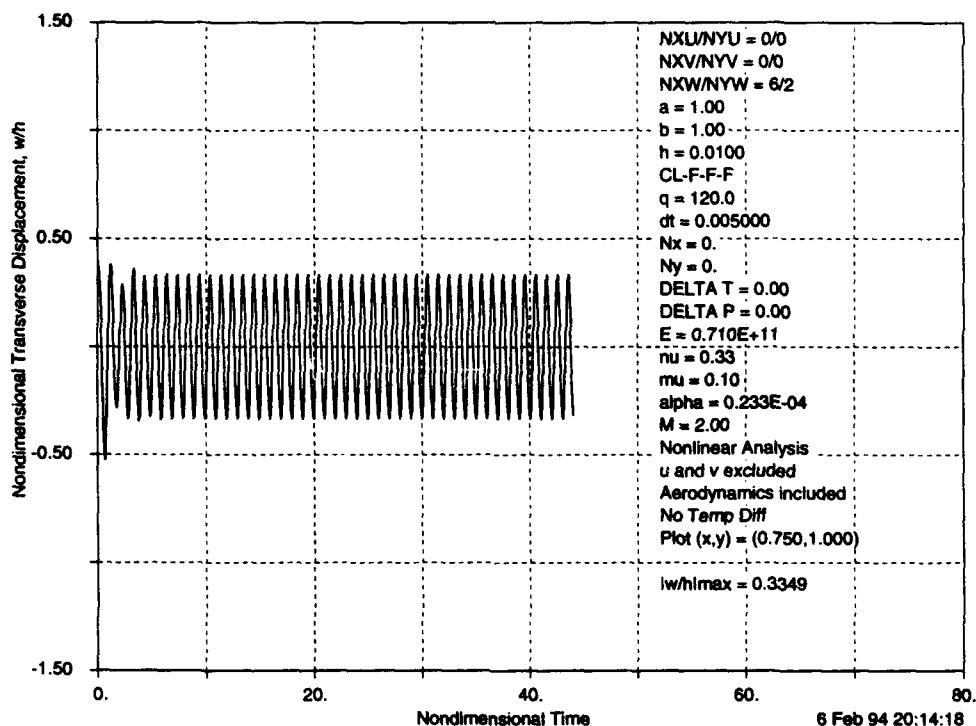


Figure 15d Transverse time history of location (0.75,1.00) where  $\lambda=120$  and  $a/b = 1$  and the in-plane motion is restricted.

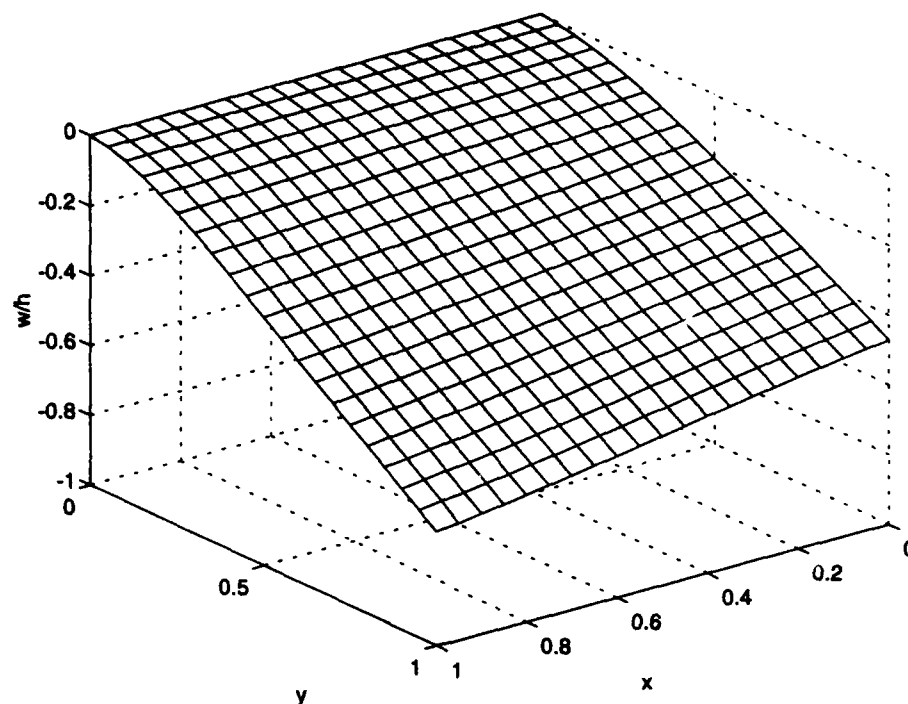


Figure 16 Panel flutter mode shape when  $\lambda=120$  ( $a/b = 1$ ).

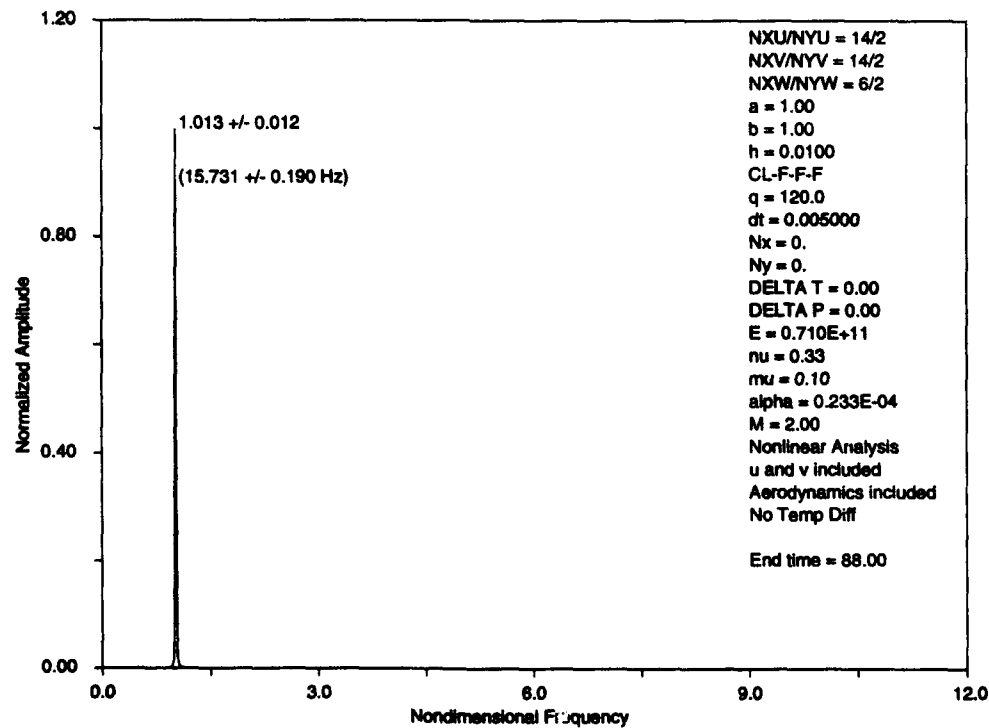


Figure 17 Power spectral density plot based on location (0.75,1.00) where  $\lambda=120$  ( $a/b = 1$ ).

frequencies whose normalized amplitude is greater than 0.05 are printed next to their peaks in the PSD plot. The dimensional frequency of the largest peak is printed in the plot enclosed in parentheses and is calculated using the nominal dimensions and parameters given previously for this example. Note in Figure 17 the nondimensional frequency is 1.013 and the dimensional frequency is 15.731 Hz.

A modified Poincaré plot of the transverse response at (0.75,1.00) is given in Figure 18. Each point in this figure represents a moment in the oscillation of the panel when the transverse velocity at (0.75,1.00) is zero and the transverse displacement amplitude at the same location is at its local maximum positive value. This figure indicates that the panel is oscillating at a single frequency and constant amplitude since the points in the modified Poincaré plot lie on a single, straight, horizontal line once the transients have decayed.

The phase plane plot, Figure 19, shows the transverse displacement versus the transverse velocity as time increases. This figure displays the panel settling into a sinusoidal oscillation about  $z = 0$  because the curve formed by the displacement/velocity pairs is an ellipse that is centered on the origin.

Figure 20 shows the time history of the average of consecutive transverse peaks. The curve in this figure describes the point about which the panel is oscillating. This figure reaffirms that the panel is oscillating about  $z = 0$ .

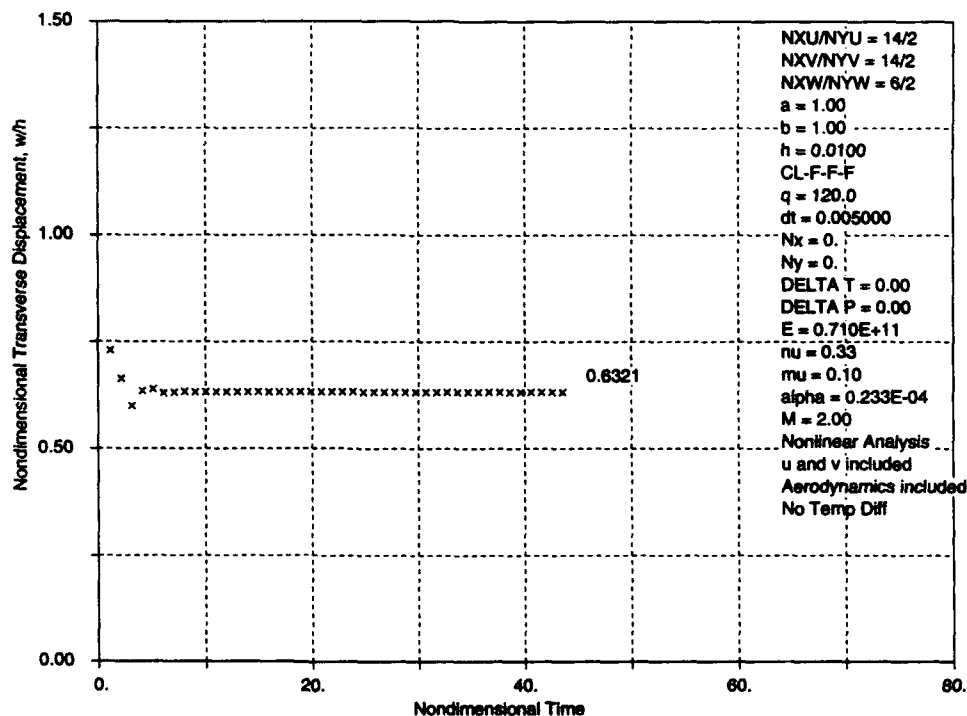


Figure 18 Modified Poincaré plot based on location (0.75,1.00) where  $\lambda=120$  ( $a/b = 1$ ).

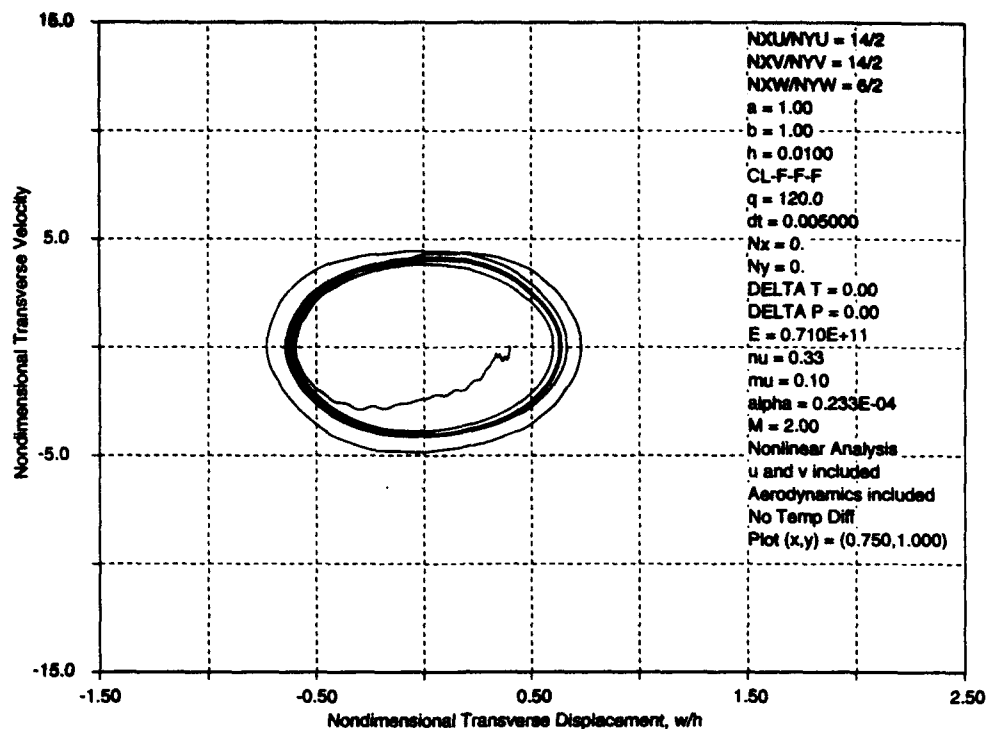


Figure 19 Phase plane plot based on location (0.75,1.00) where  $\lambda=120$  ( $a/b = 1$ ).

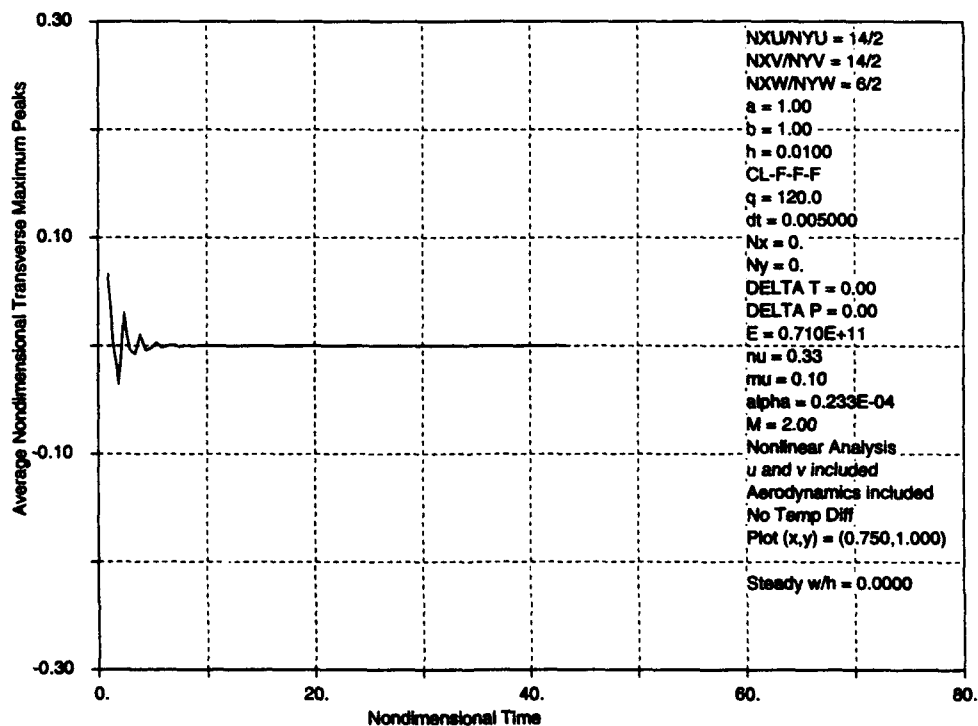


Figure 20 Average transverse peak amplitude based on location (0.75,1.00) where  $\lambda=120$  ( $a/b = 1$ ).

Figures 21a and b show the contributions of the  $\bar{c}_{i1}$  and  $\bar{c}_{i2}$  transverse modes, respectively, to the flutter mode shown in Figure 16. Figure 21a indicates that the first two transverse modes in the  $x$  direction contribute much more to the flutter mode shape than the latter four modes, but recall from Figure 2 that all six modes are required to form an accurate solution. The plot in Figure 21b indicates that the first transverse mode in the  $y$  direction contributes more than ten times that of the second mode to form the flutter mode.

The converged  $a/b = 1$  curve in Figure 11 stopped at  $\lambda=400$  because the response for higher nondimensional dynamic pressures becomes more nonlinear. As the dynamic pressure increases above  $\lambda=400$ , the response transitions from oscillating about some point other than zero to beating and then to nonperiodic. Figures 22-28, 29-34, and 35-40 show examples of the panel response when  $\lambda=500$ , 640 (beating), and 700 (nonperiodic) respectively.

Figures 22-28 display the panel response when it oscillates about some point other than zero. Figures 22a-c show the  $\bar{u}$ ,  $\bar{v}$ , and  $\bar{w}$  displacements as time increases. Note that the in-plane displacements are beating and the transverse displacement is oscillating sinusoidally. The smaller negative peaks in Figure 22a correspond to the maximum positive transverse displacements and the larger negative peaks correspond to the maximum negative transverse displacements. This figure indicates that the in-plane displacement of the outboard three-quarter chord point does not move in the positive  $x$  direction under these flow conditions. Figure 22b shows the panel is oscillating such that its outboard edge has positive and negative displacement

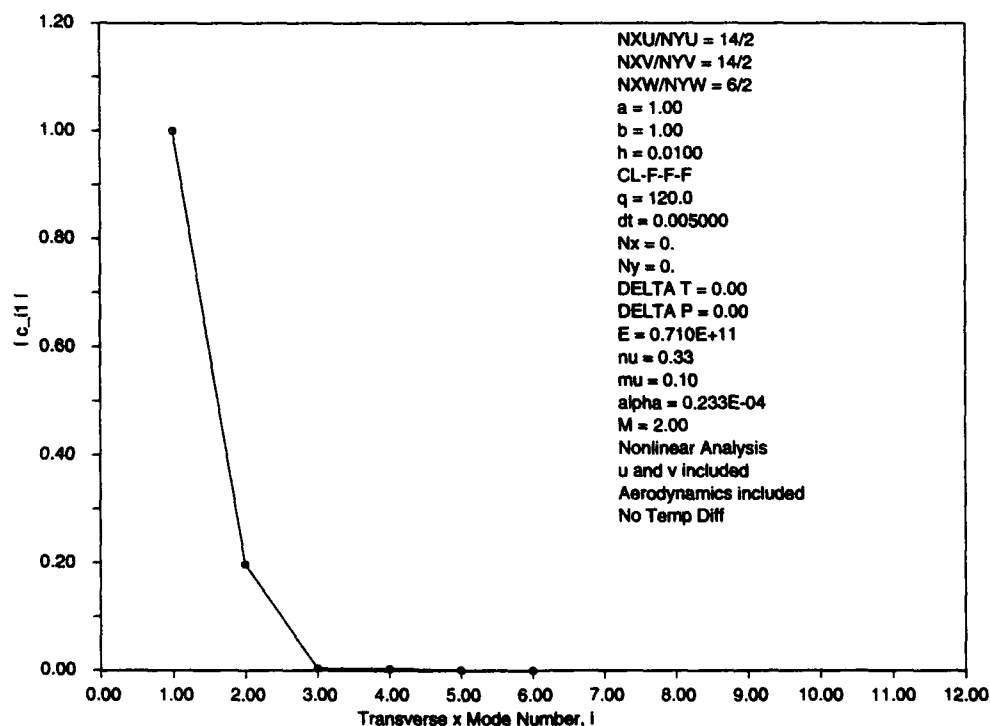


Figure 21a Chordwise transverse modal contribution plot where  $\lambda=120$  ( $a/b = 1$ ).

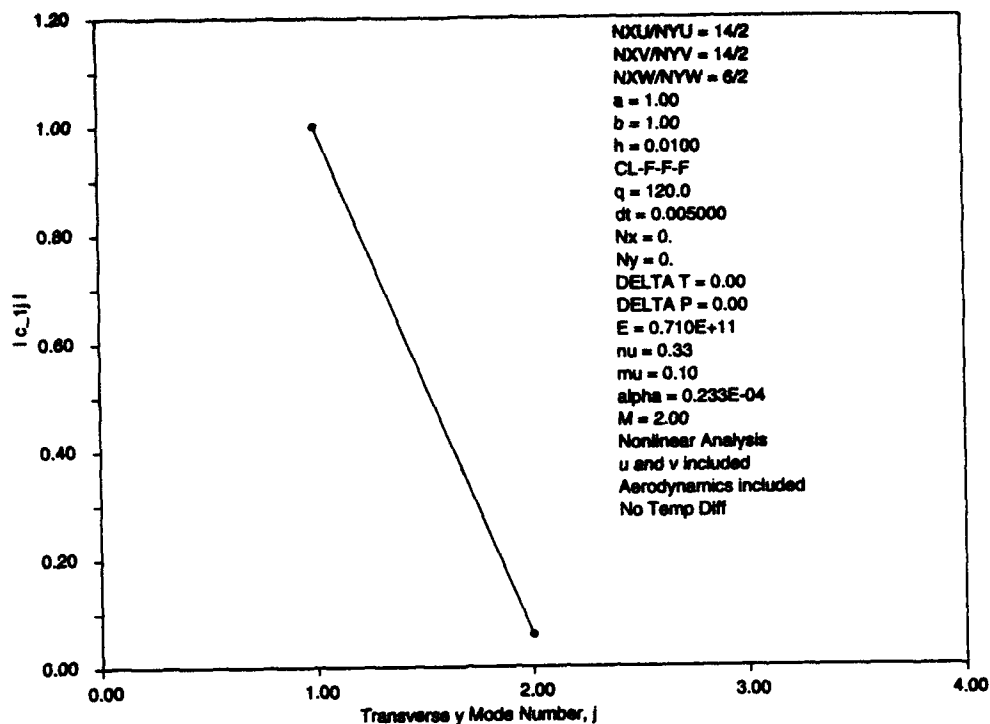


Figure 21b Spanwise transverse modal contribution plot where  $\lambda=120$  ( $a/b = 1$ ).

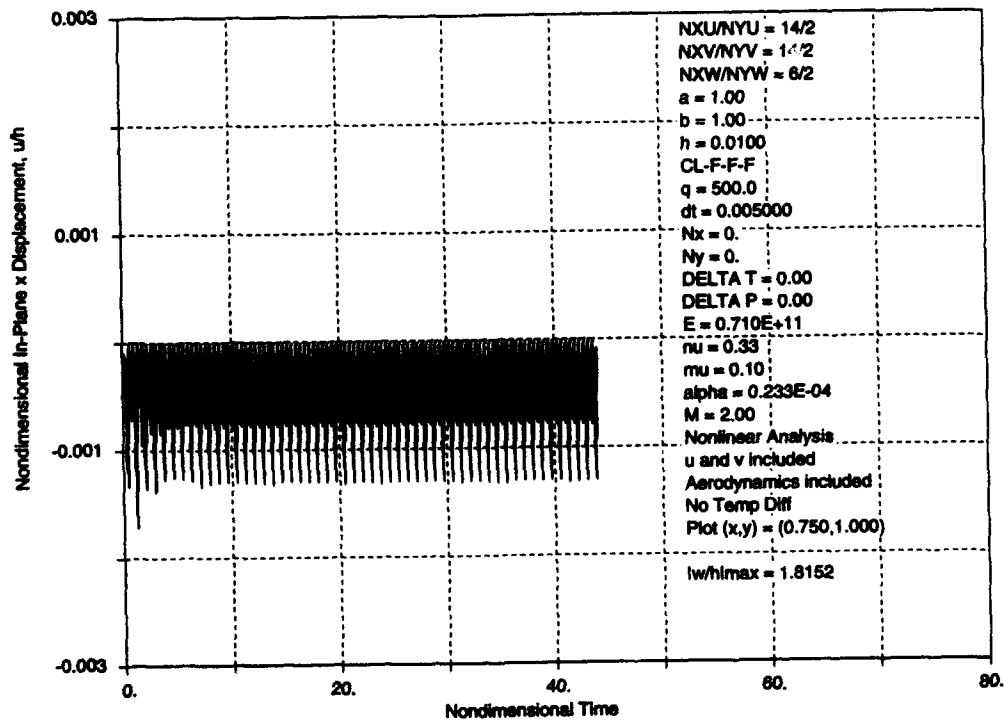


Figure 22a In-plane time history in the x direction of point (0.75,1.00) where  $\lambda=500$  ( $a/b = 1$ ).

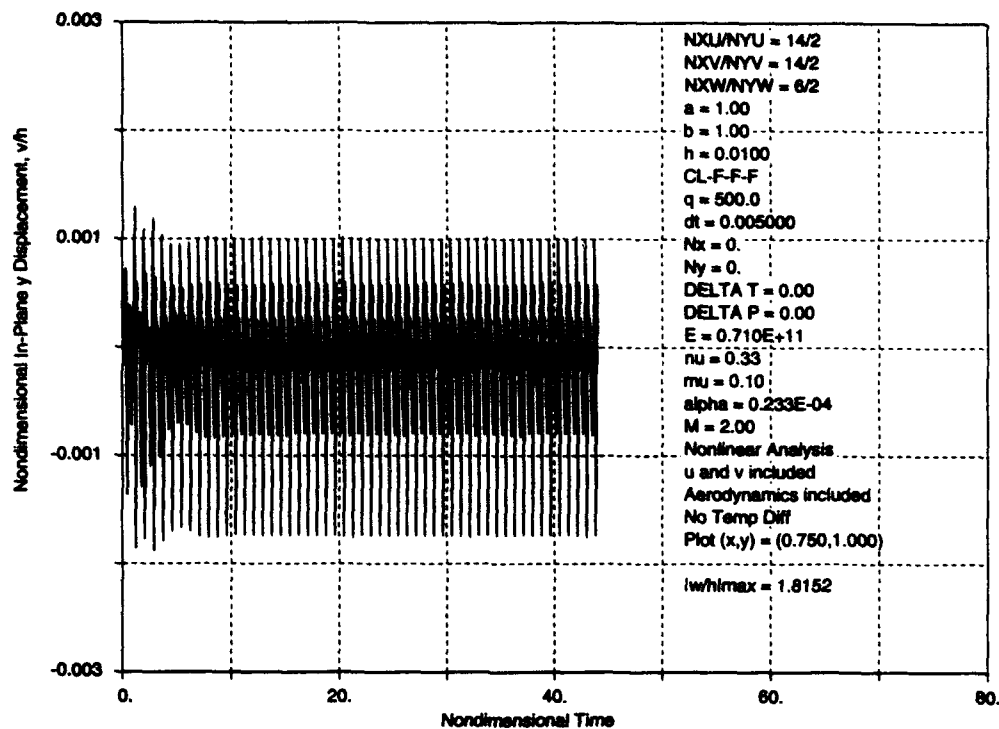


Figure 22b In-plane time history in the y direction of point (0.75,1.00) where  $\lambda=500$  ( $a/b = 1$ ).

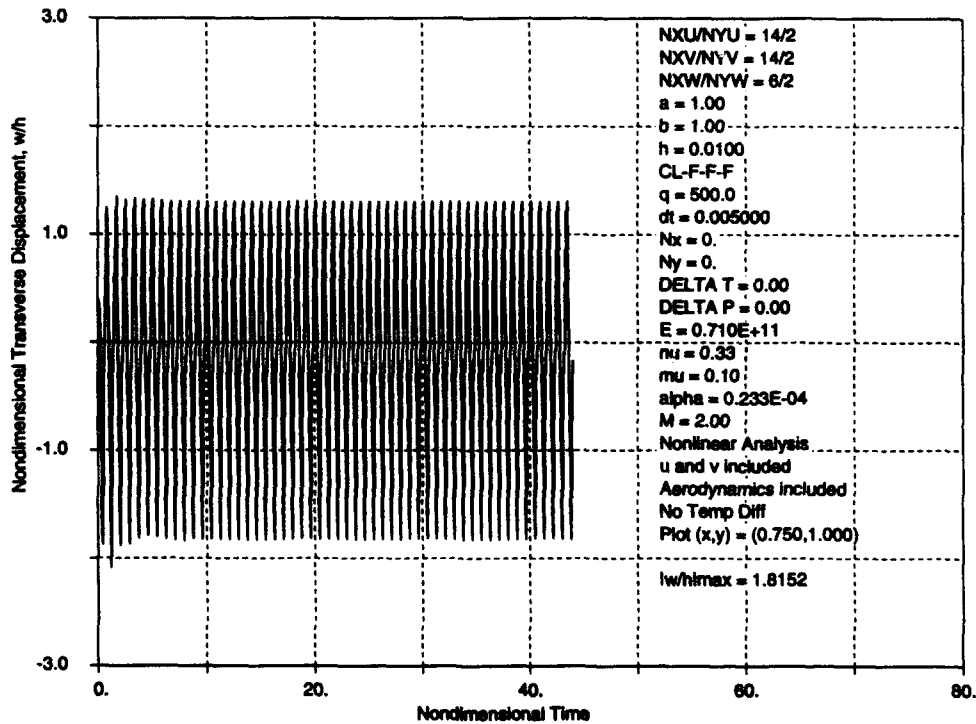


Figure 22c Transverse time history of location (0.75,1.00) where  $\lambda=500$  ( $a/b = 1$ ).

values in the  $y$  direction. The positive displacement in the  $y$  direction of this location indicates that the panel is expanding at these conditions also. Figure 22c shows the nondimensional transverse displacement in time. A visual inspection of this figure shows that the point on the panel being investigated is oscillating about some point other than zero. This phenomenon was mentioned in Reference 7, Figure 19, where the author states there is a response that has "different peak amplitudes." (Reference 7 documents the postflutter response of a panel that is simply supported on all four sides.)

A three-dimensional plot of the panel at one of the steady state peaks in Figure 22c is given in Figure 23. Note in this figure that the outboard edge of the panel is deflected more than any other constant span slice through the panel and the aftermost point on the outboard edge is deflected more than any other point on the panel. The slope along the outboard edge increases between approximately  $a/3$  and  $2a/3$  such that the slope over the leading third is one constant and that over the trailing third is a greater constant.

Figure 24 contains the power spectral density plot that was created using the nondimensional transverse response at location (0.75,1.00). Note that the response is predominantly single mode driven with three higher harmonic modes beginning to appear. The predominant oscillation frequency, 18.6 Hz, is lower than the oscillation frequency when  $\lambda=400$ .

The modified Poincaré and phase plane plots, Figures 25 and 26, show that the panel initial deformations decay to a periodic oscillation in time when subject to these flow conditions. Note

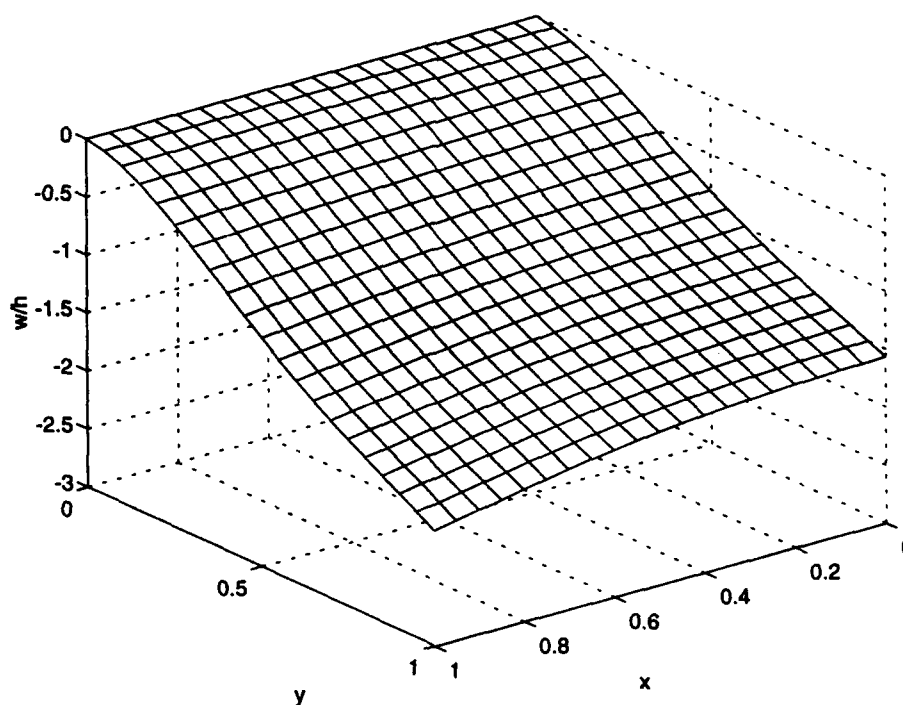


Figure 23 Panel flutter mode shape when  $\lambda=500$  ( $a/b = 1$ ).



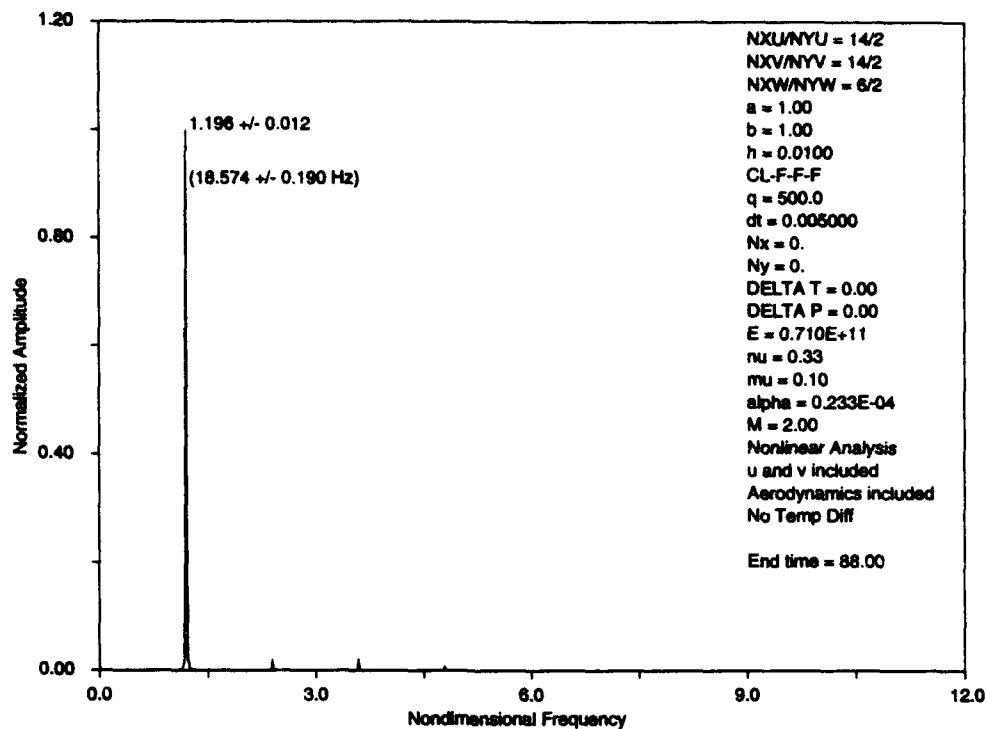


Figure 24 Power spectral density plot based on location (0.75,1.00) where  $\lambda=500$  ( $a/b = 1$ ).

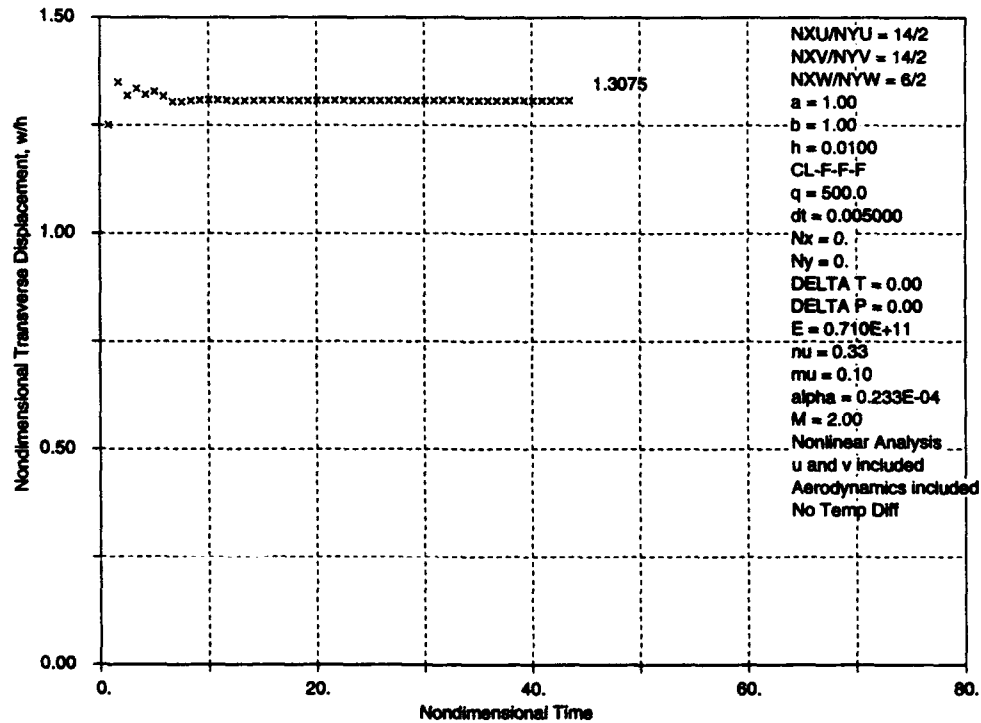


Figure 25 Modified Poincaré plot based on location (0.75,1.00) where  $\lambda=500$  ( $a/b = 1$ ).

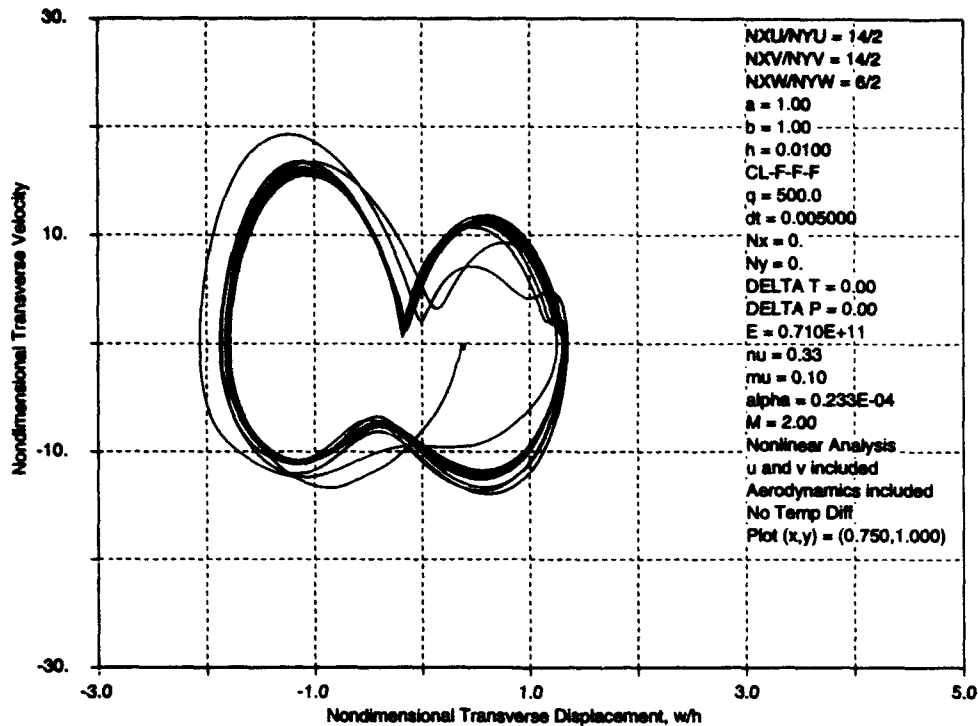


Figure 26 Phase plane plot based on location (0.75,1.00) where  $\lambda=500$  ( $a/b = 1$ ).

that the points in the Poincaré plot lie on one straight line and phase plane steady state curve is no longer an ellipse.

The time history of the average of consecutive transverse peaks at location (0.75,1.00) is shown in Figure 27. It indicates that the panel is oscillating about  $z = -0.2689$ .

Figures 28a and b show the contribution of the transverse  $x$  and  $y$  modes to the flutter mode shown in Figure 23 based on the transverse response at (0.75,1.00). Figure 28a indicates that the first three modes contribute more than the last three. Comparing this figure to Figure 21a shows the second mode contributes less and the third mode contributes more at this nondimensional dynamic pressure than when  $\lambda=120$ . Comparing Figure 21b to Figure 28b shows that the second mode in the  $y$  direction contributes more when  $\lambda=500$  than it did when  $\lambda=120$ .

Figures 29a-c exhibit the nondimensional in-plane  $x$  and  $y$  and transverse displacement time histories, respectively, of location (0.75,1.00) where  $\lambda=640$ . All three time histories display trends indicative of beating. The evaluation point moves in the negative  $x$  direction only and in both the positive and negative  $y$  directions as in the previous cases. A visual inspection of Figure 29c indicates that the panel is not oscillating about  $z = 0$ .

The panel is in the shape shown in Figure 30 when it reaches one of the maximum steady state transverse peaks. In this case, the outboard edge is deflected upwards such that the first

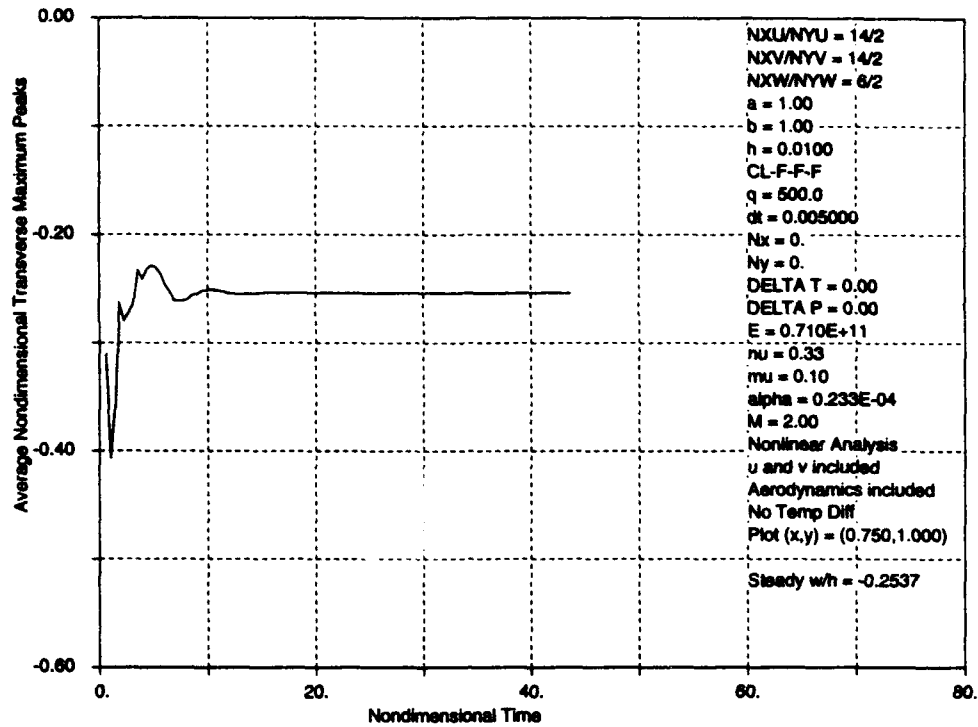


Figure 27 Average transverse peak amplitude based on location (0.75,1.00) where  $\lambda=500$  ( $a/b = 1$ ).

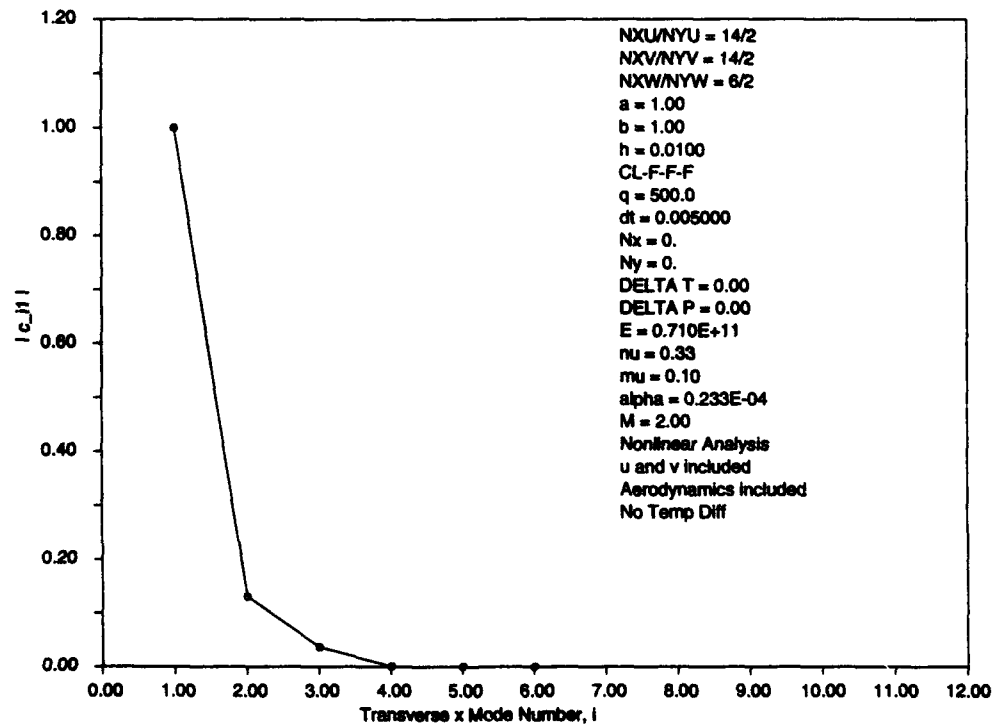


Figure 28a Chordwise transverse modal contribution plot where  $\lambda=500$  ( $a/b = 1$ ).

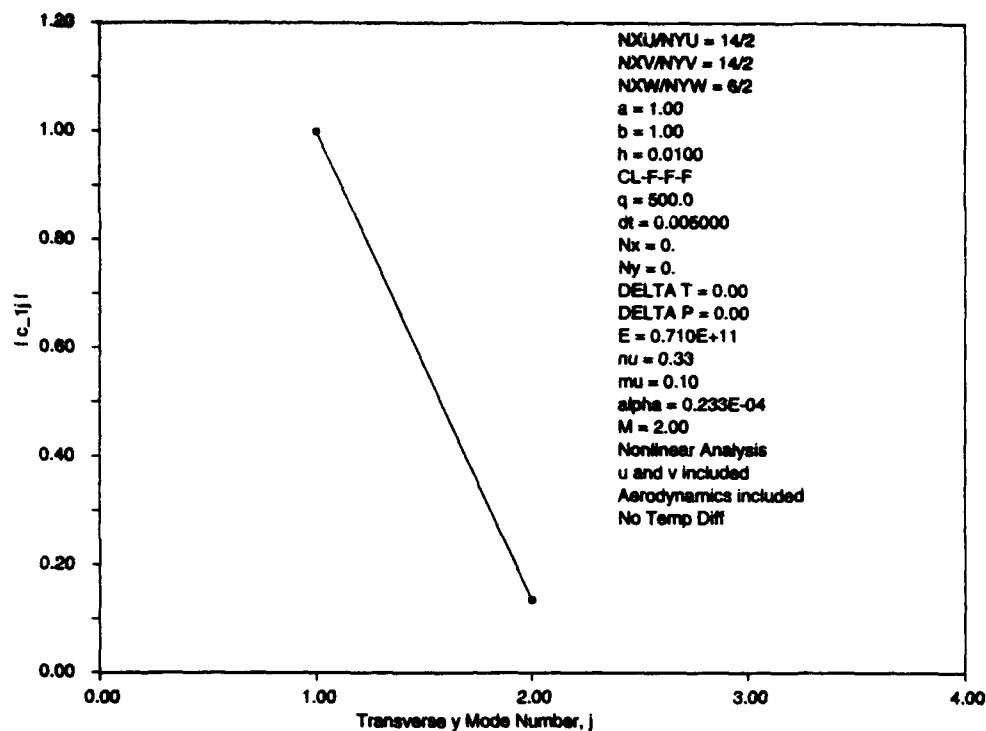


Figure 28b Spanwise transverse modal contribution plot where  $\lambda=500$  ( $a/b = 1$ ).

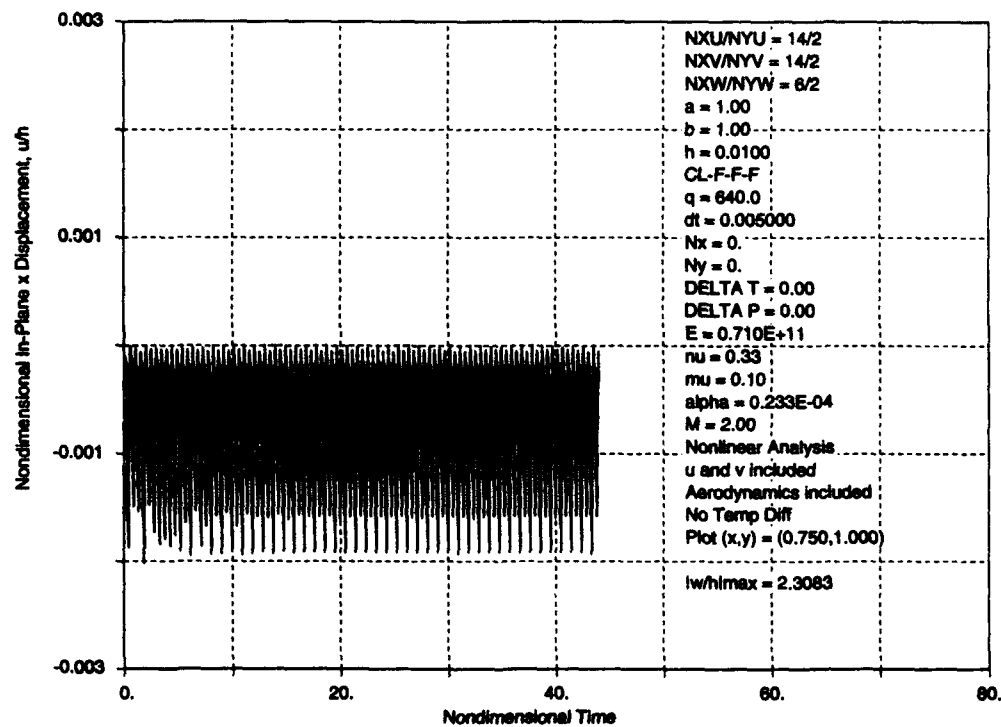


Figure 29a In-plane time history in the x direction of point (0.75,1.00) where  $\lambda=640$  ( $a/b = 1$ ).

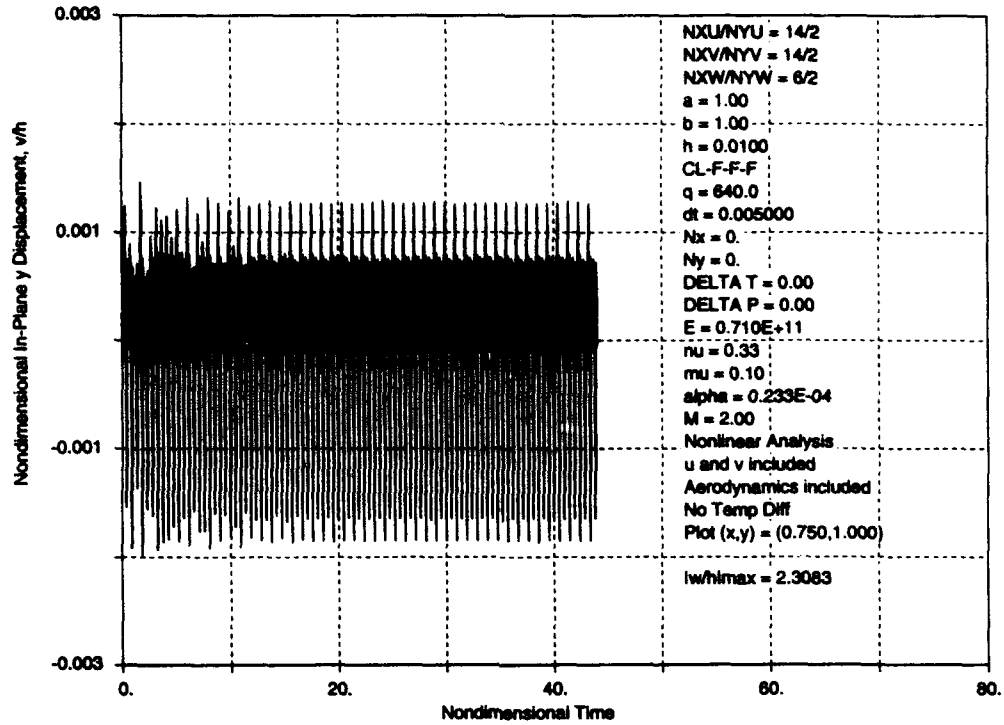


Figure 29b In-plane time history in the y direction of point (0.75,1.00) where  $\lambda=640$  ( $a/b = 1$ ).

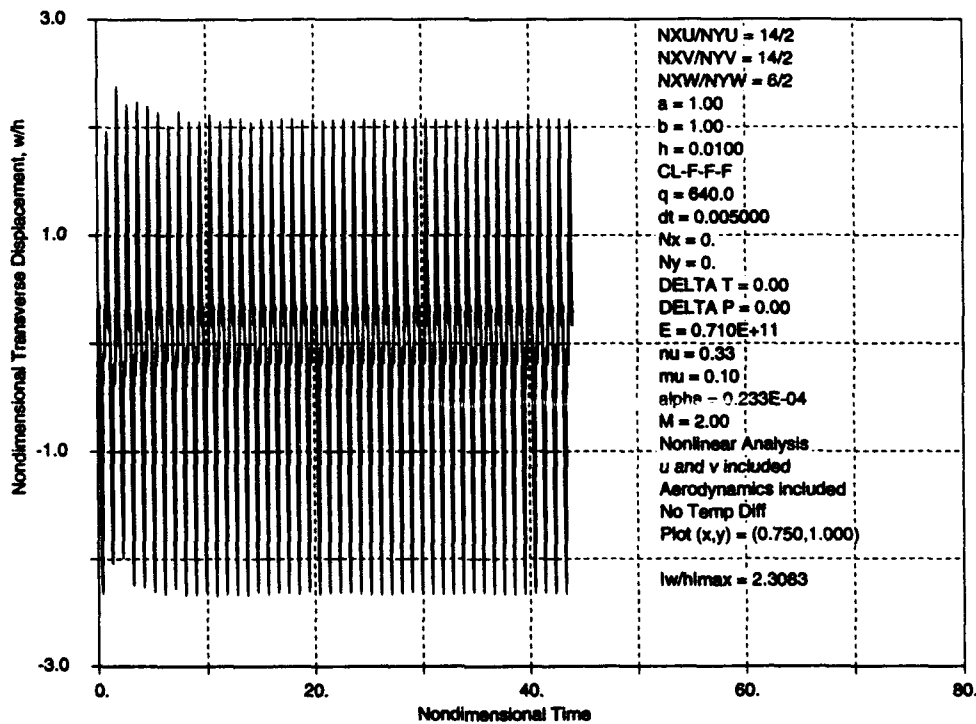


Figure 29c Transverse time history of location (0.75,1.00) where  $\lambda=640$  ( $a/b = 1$ ).

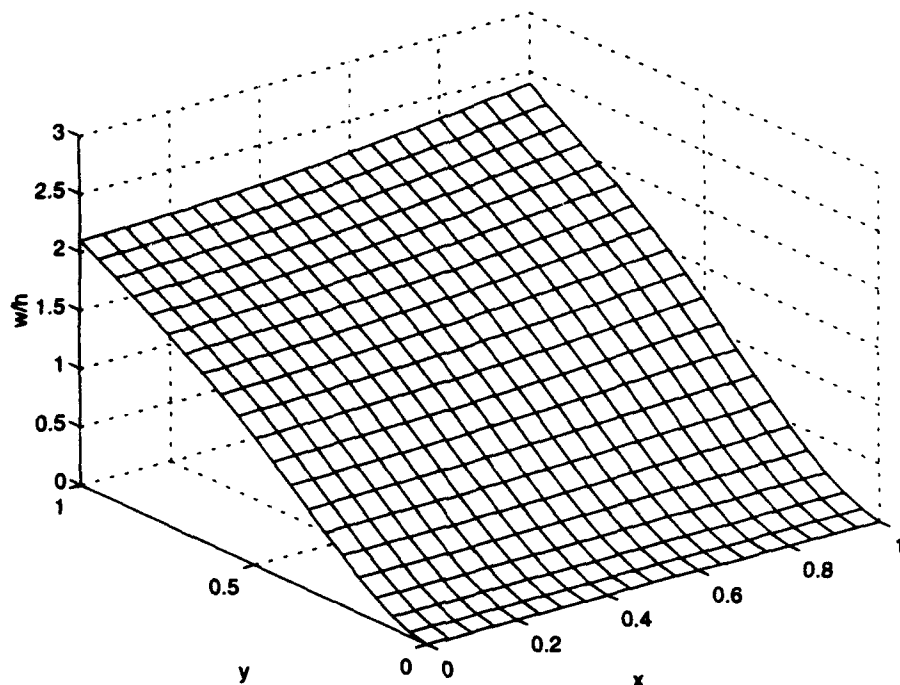


Figure 30 Panel flutter mode shape when  $\lambda=640$  ( $a/b = 1$ ).

30% of the outboard chord is at a constant slope and the last 40% is at a greater slope with a smooth variation between.

Figure 31 displays the PSD plot derived from the transverse response. Note that the panel oscillation is composed primarily of two frequencies, the higher of which is the third harmonic of the first.

The modified Poincaré plot of the transverse response of location (0.75,1.00) where  $\lambda=640$  is provided in Figure 32. The loci of points make three straight horizontal lines which means that there are three points within one oscillation cycle at which the transverse velocity is zero and the displacement is a maximum with respect to the local time history. Close examination of Figure 29a shows three local peaks within one cycle.

The plot in Figure 33 is the phase plane plot of the transverse response. The phase plane curve contains two steady state loops that are due to the secondary peaks within the oscillation cycle. The average consecutive time history peak plot is not shown for this  $\lambda$  case because it shows an oscillating curve due to the secondary peaks. It is omitted because it does not provide additional information.

The transverse modal contribution plots are included as Figures 34a and b. As in the  $\lambda=500$  case, the first three transverse modes in the  $x$  direction contribute more to the flutter mode

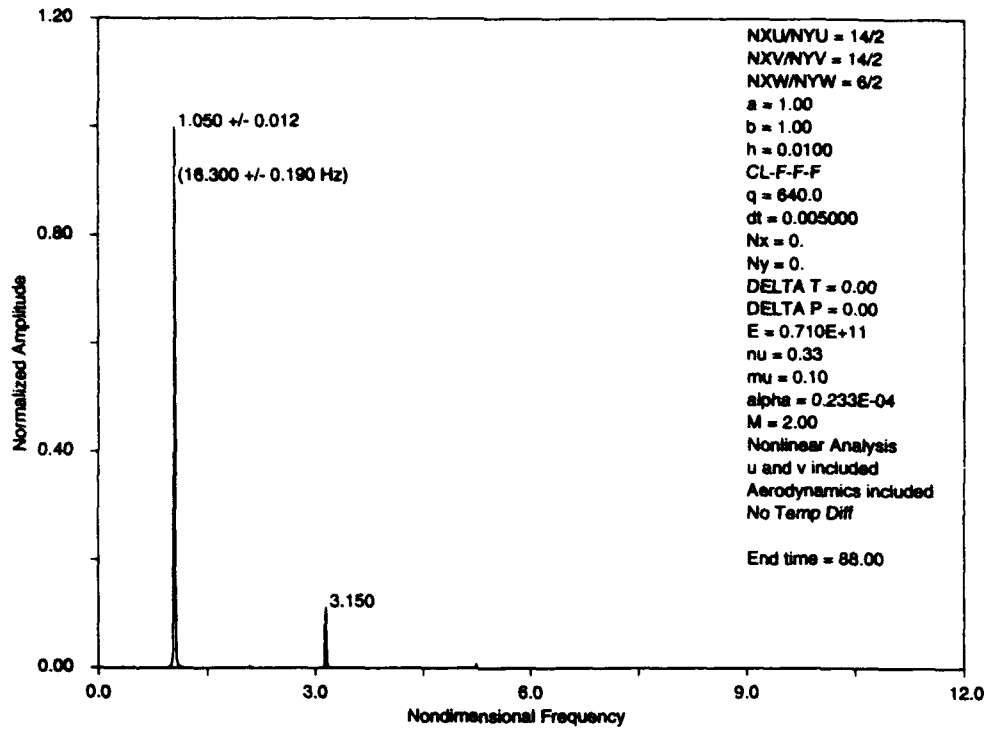


Figure 31 Power spectral density plot based on location (0.75,1.00) where  $\lambda=640$  ( $a/b = 1$ ).

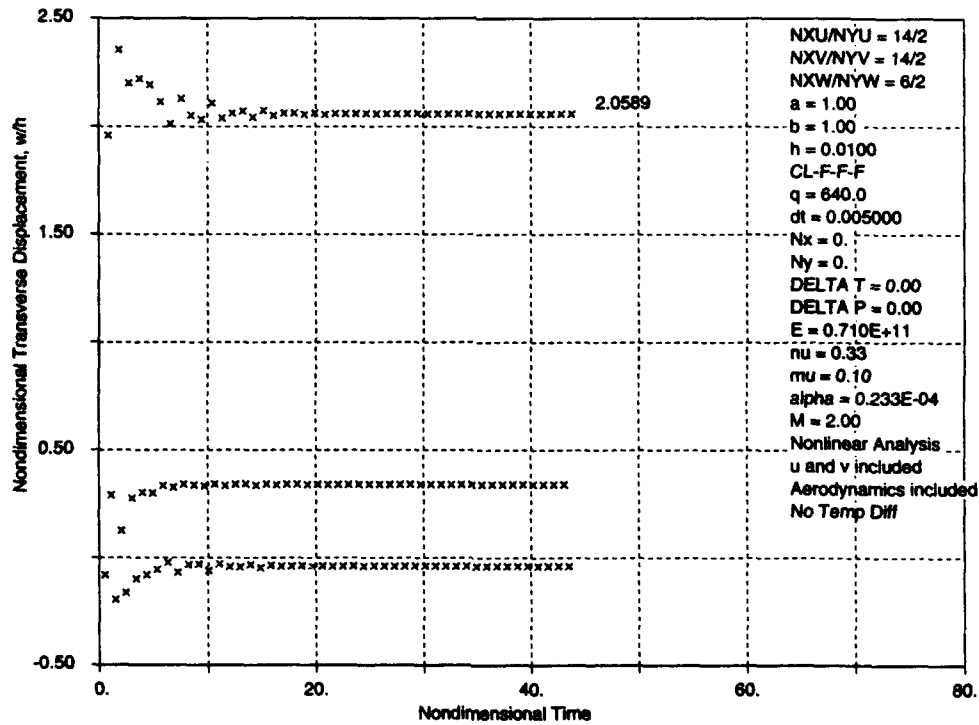


Figure 32 Modified Poincaré plot based on location (0.75,1.00) where  $\lambda=640$  ( $a/b = 1$ ).

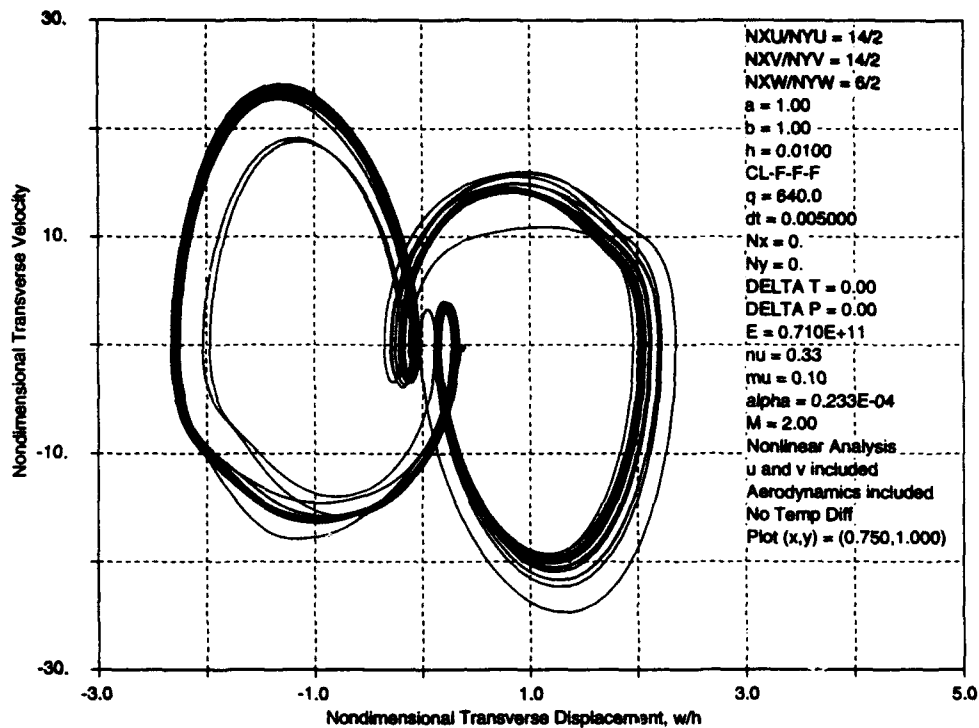


Figure 33 Phase plane plot based on location (0.75,1.00) where  $\lambda=640$  ( $a/b = 1$ ).

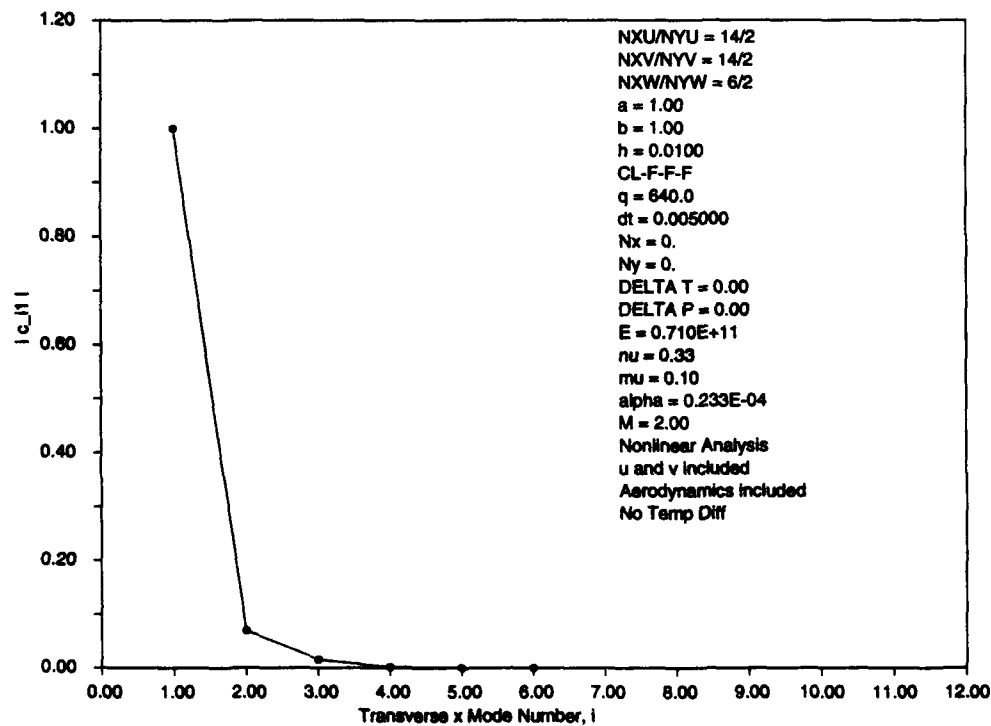


Figure 34a Chordwise transverse modal contribution plot where  $\lambda=640$  ( $a/b = 1$ ).



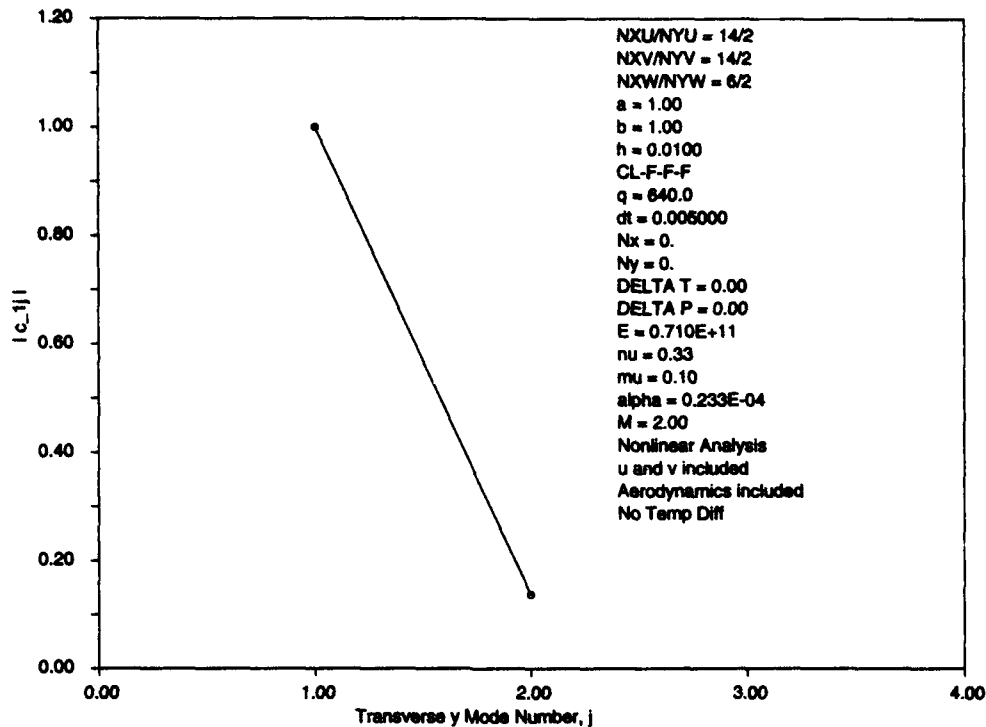


Figure 34b Spanwise transverse modal contribution plot where  $\lambda=640$  ( $a/b = 1$ ).

shape than do the last three modes, but in this case the second and third modes contribute less than they did in the  $\lambda=500$  case. Comparing Figures 28b and 34b shows no change in the transverse y modal contribution.

Figures 35-40 show a nonperiodic panel response where  $\lambda=700$ . Figures 35a, b, and c present the  $\bar{u}$ ,  $\bar{v}$ , and  $\bar{w}$  time histories at location (0.75,1.00). Note that the response in each figure is nonperiodic. The in-plane displacement in the x direction is still never positive and the in-plane displacement in the y direction is both positive and negative. Figure 36 shows the shape of the panel at one of the later transverse time history peaks. The panel shape is similar to that when  $\lambda=640$  except the deflection is greater. Figure 37 shows the power spectral density plot based on the transverse response at location (0.75,1.00). It demonstrates that there are many modes interacting to form the response at  $\lambda=700$ . The Poincaré and phase plane plots are provided in Figures 38 and 39. These figures support the conclusions made based on the last five figures in that the panel response is nonperiodic. Finally, Figures 40a and b show the transverse modal contribution for the same transverse peak used to form Figure 36. The second and third modes in the x direction contribute less and the second mode in the y direction contributes more than those when  $\lambda=640$ .

#### Initial Condition Variation

The steady state response of nonlinear systems is dependent upon the initial conditions (ICs) used to initiate the oscillations within the structure. All the previous figures were created

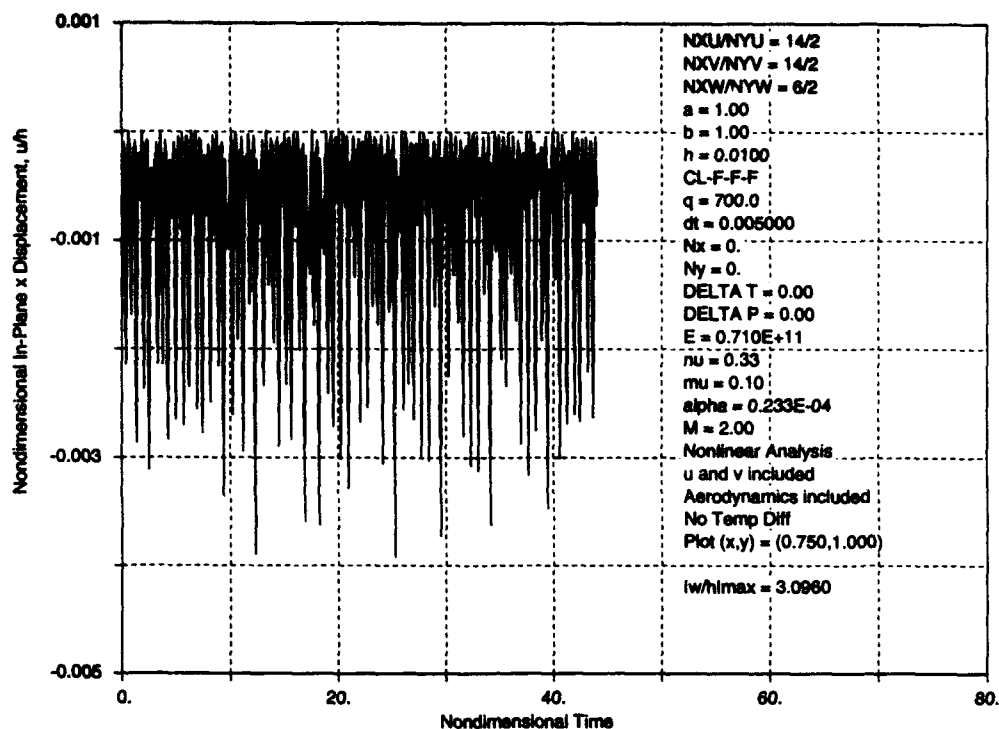


Figure 35a In-plane time history in the  $x$  direction of point (0.75,1.00) where  $\lambda=700$  ( $a/b = 1$ ).

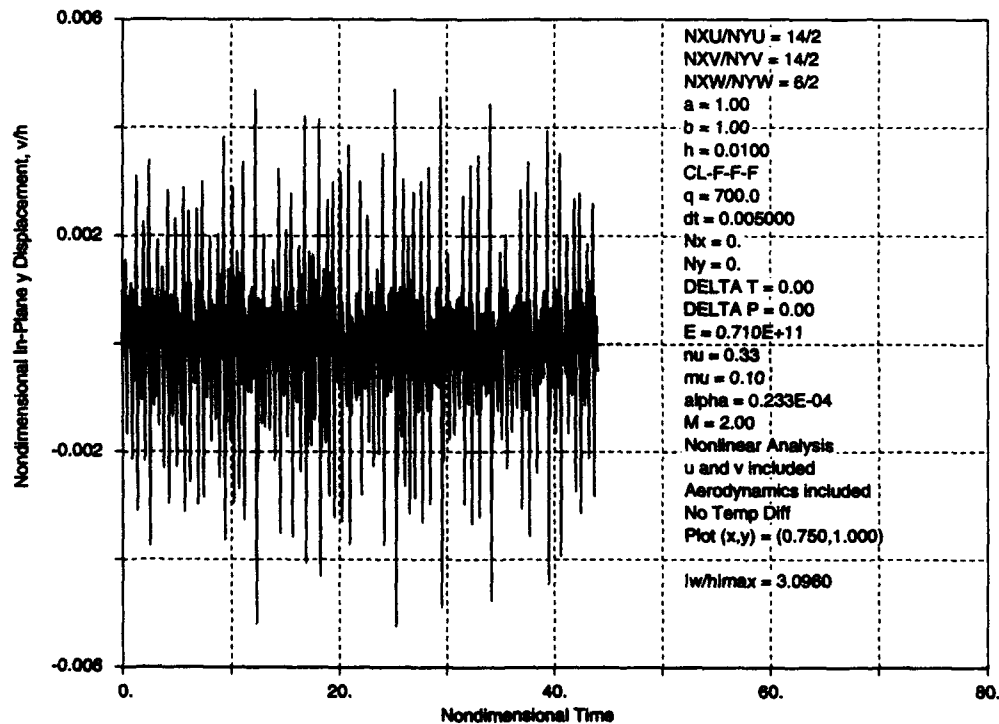


Figure 35b In-plane time history in the  $y$  direction of point (0.75,1.00) where  $\lambda=700$  ( $a/b = 1$ ).

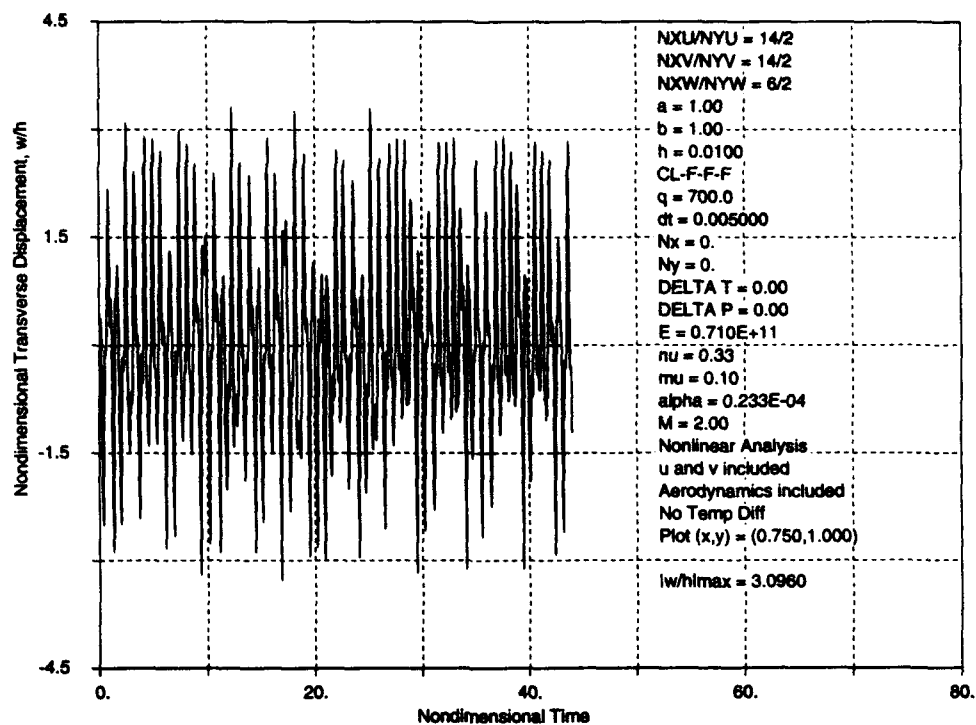


Figure 35c Transverse time history of location (0.75,1.00) where  $\lambda=700$  ( $a/b = 1$ ).

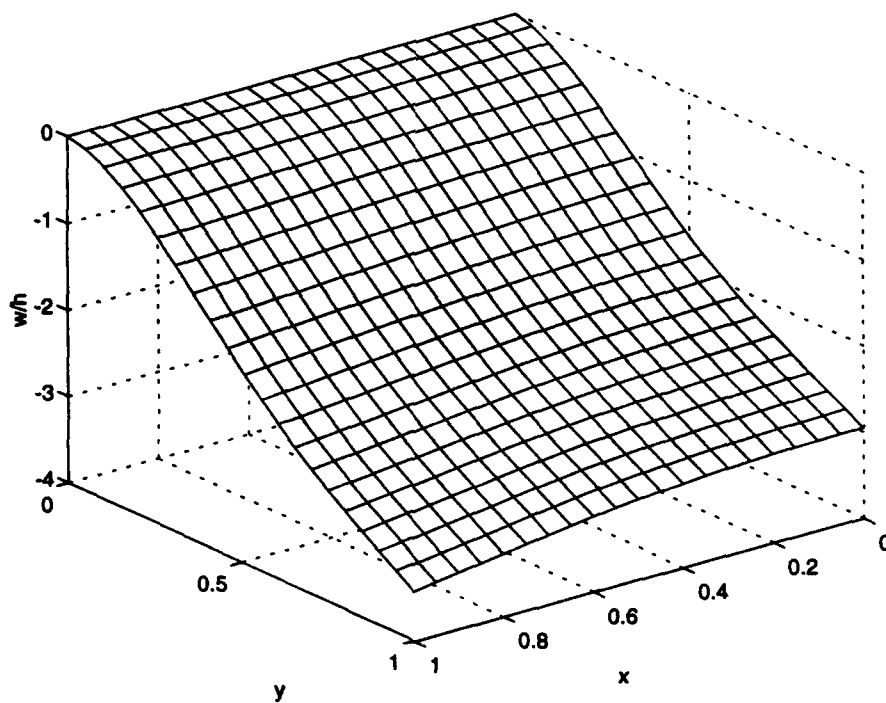


Figure 36 Panel flutter mode shape when  $\lambda=700$  ( $a/b = 1$ ).

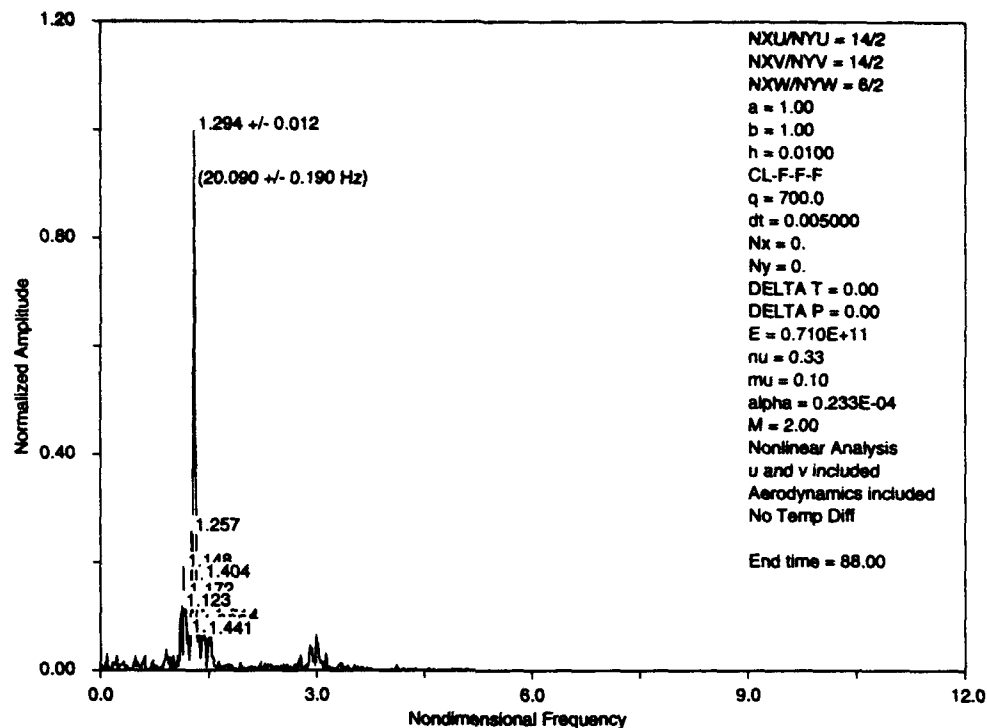


Figure 37 Power spectral density plot based on location (0.75,1.00) where  $\lambda=700$  ( $a/b = 1$ ).

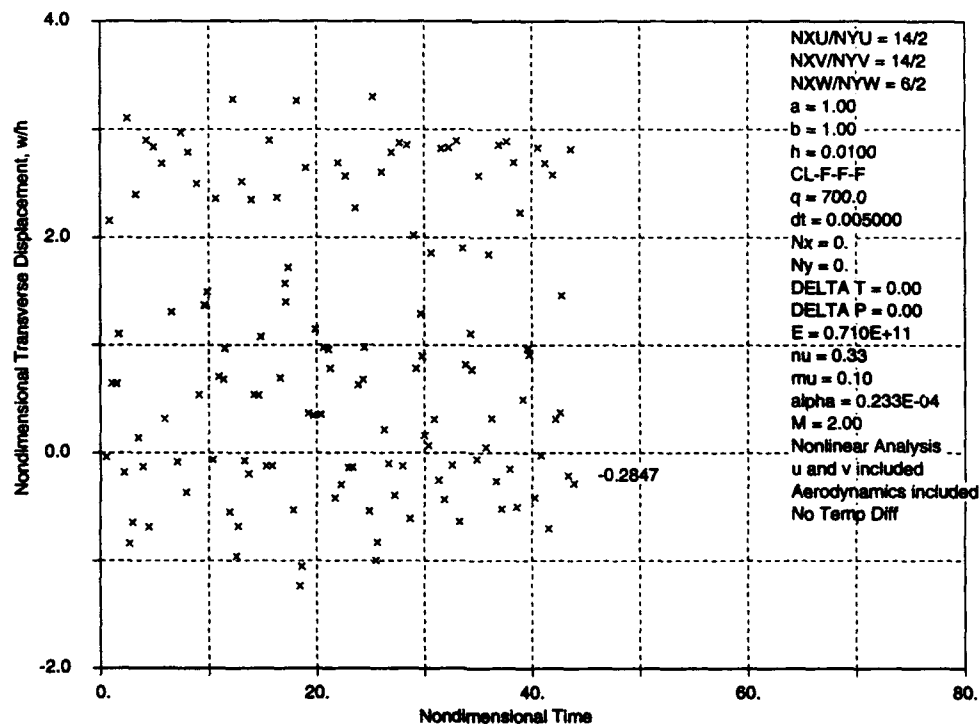


Figure 38 Modified Poincaré plot based on location (0.75,1.00) where  $\lambda=700$  ( $a/b = 1$ ).

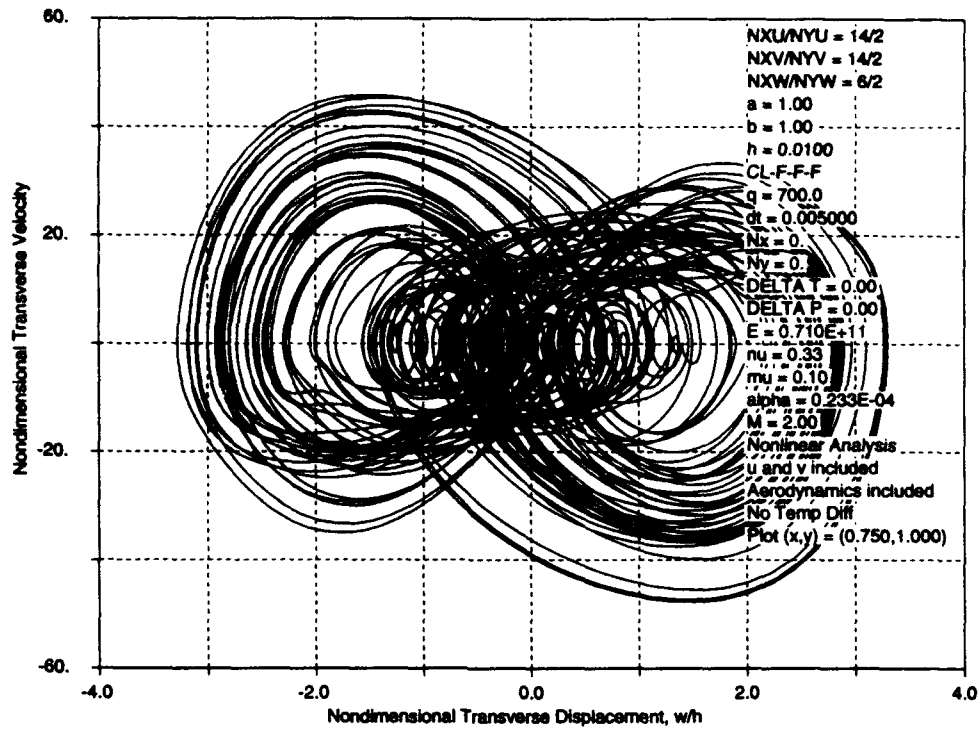


Figure 39 Phase plane plot based on location (0.75,1.00) where  $\lambda=700$  ( $a/b = 1$ ).

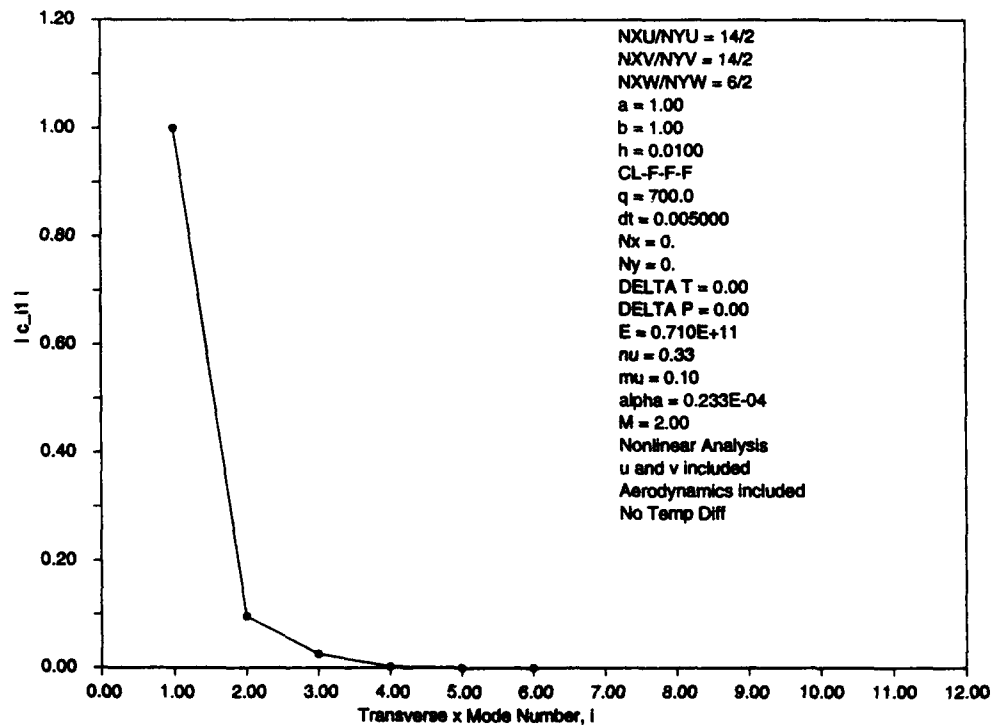


Figure 40a Chordwise transverse modal contribution plot where  $\lambda=700$  ( $a/b = 1$ ).

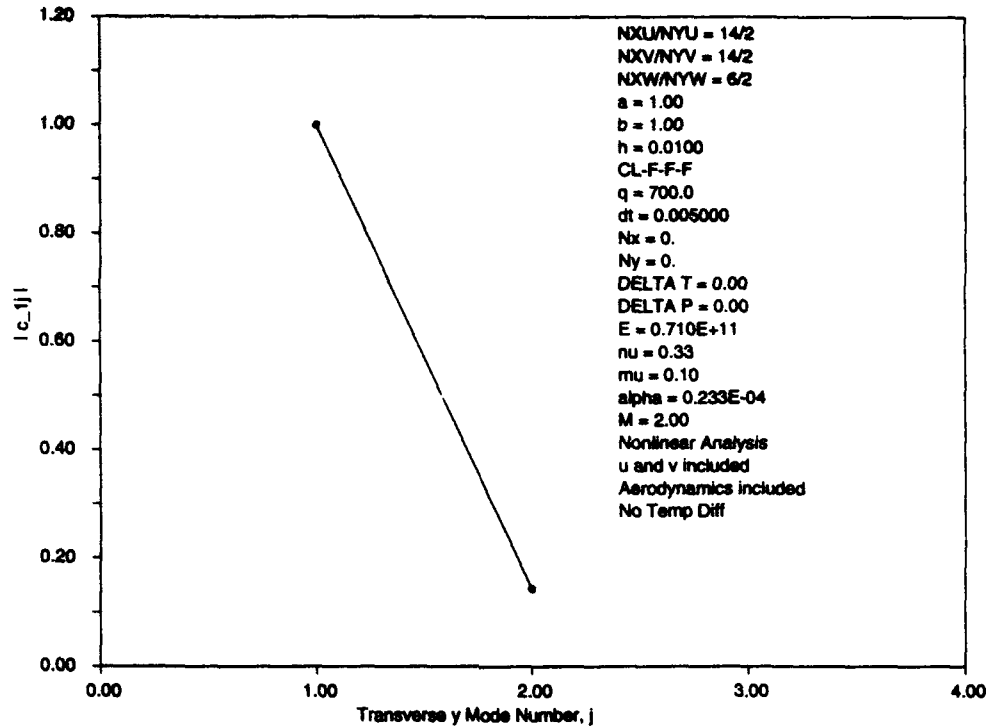


Figure 40b Spanwise transverse modal contribution plot where  $\lambda=700$  ( $a/b = 1$ ).

using the results of analyses started with the ICs given at the end of Section II, (10). The following two ICs were investigated to determine their effect on the steady state response. In all cases, the initial transverse velocity was zero.

$$\bar{c}_{11} = -0.001 / h \quad (11)$$

$$\bar{c}_{11} = 0.002 / h \quad (12)$$

The negative IC, (11), was employed to determine if the buckled transverse response would oscillate about the same buckled position, about the opposite sign, same magnitude buckled position, or about some new equilibrium. The  $\lambda=500$  flow condition was investigated with these ICs. The in-plane responses are not different, but the transverse response indicates that the panel oscillates about the opposite sign, same magnitude buckled position as shown in Figure 41. In fact, the transverse response is a mirror image of the response shown in Figure 22c about the  $w = 0$  axis. Since the transverse response only changed its sign, the in-plane responses should not show any change because the in-plane equations of motion are dependent upon the square of the transverse generalized coordinate only.

Doubling the ICs, employing IC (12), does not affect the steady state transverse response other than slightly increasing the transient decay time. The transverse response to the IC outlined in (12) is shown in Figure 42.

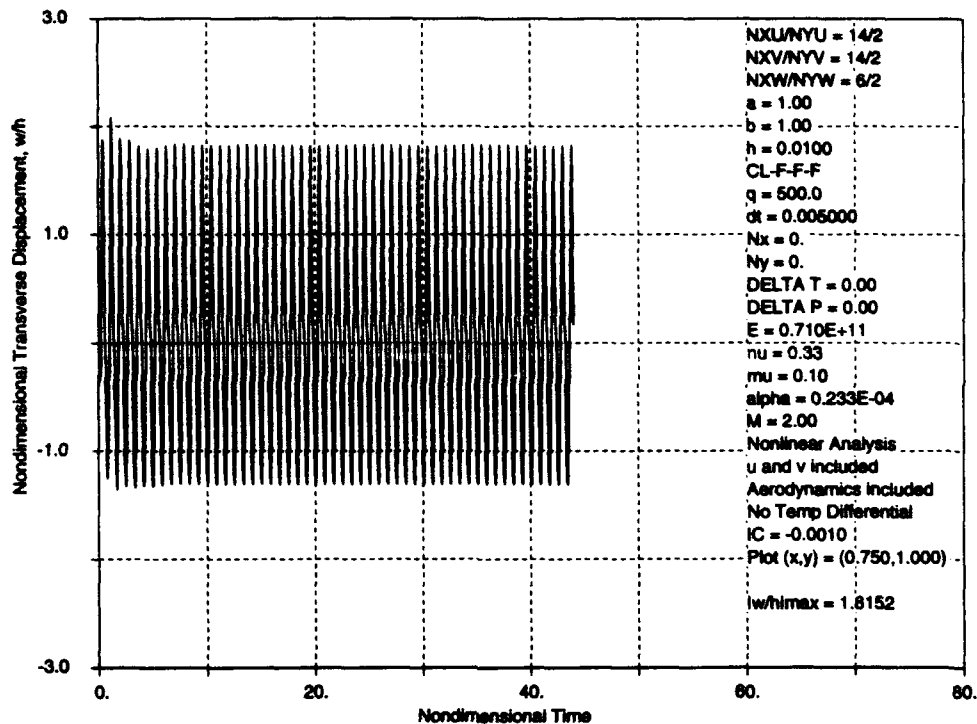


Figure 41 Transverse time history of location (0.75,1.00) where  $\lambda=500$  and employing the initial conditions outline in Expression (11) ( $a/b = 1$ ).

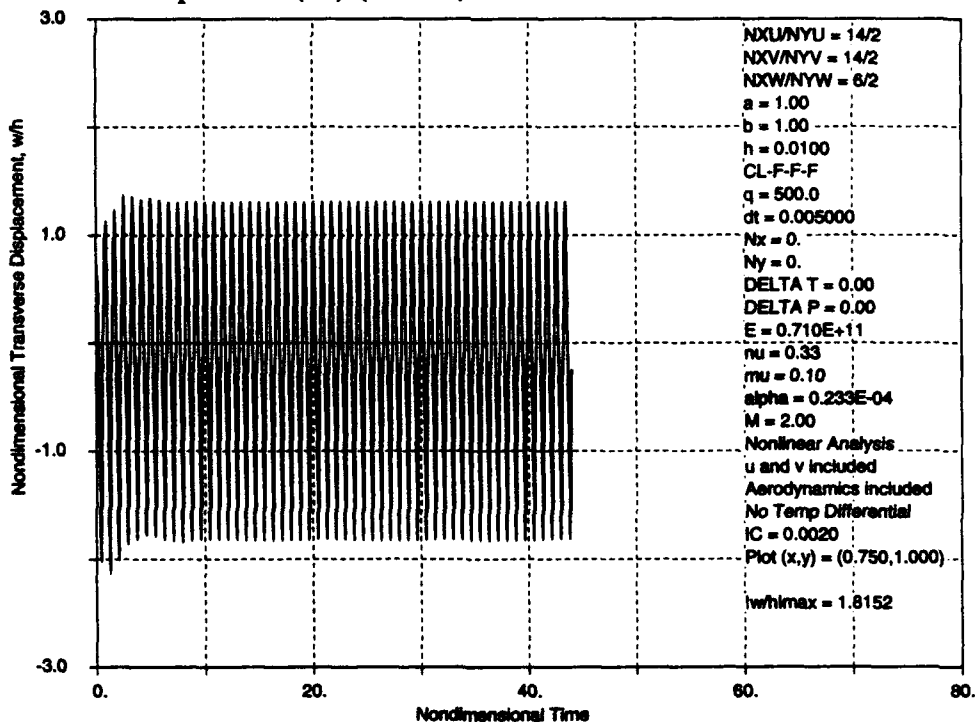


Figure 42 Transverse time history of location (0.75,1.00) where  $\lambda=500$  and employing the initial conditions outline in Expression (12) ( $a/b = 1$ ).

## SECTION IV

### Comparison to Previous Research

Several reports were chosen from the vast number of documented panel flutter analyses to be used to substantiate the analytical and numerical results presented in this effort. Only one other paper investigates the response of cantilevered panels, Reference 1. The other reports referenced here investigated panels that are simply supported or clamped on all four sides. The simply supported panel results using this analytical procedure are included.

Weiliang and Dowell's paper (Reference 1) was the basis from which this research was generated. Their analytical procedure is followed here, but the computer program for the present effort was written so that many different panel boundary conditions could be investigated if the modal functions were known. The difference between their research and this effort is the modal convergence study performed here included the in-plane modes whereas their paper used one mode in their approximation of both in-plane displacements. The premise of this effort is that more than one in-plane mode should be incorporated to predict the postflutter response of a cantilevered panel. Recall that Figures 4, 5, and 6 present the results of the in-plane modal convergence study of an  $a/b = 1$  panel. These figures show that the maximum transverse displacement of a cantilevered panel is dependent upon the number of in-plane modes incorporated in the analysis.

A comparison between Weiliang and Dowell's work and this investigation includes the following similarities and differences:

1. The  $N_X U = N_X V = 1$  curve in Figure 4 appears to be identical to the  $m=6, n=2$  curve in Figure 6 (Reference 1) showing this work reproduced some of the Weiliang and Dowell results.
2. Figure 7a (Reference 1) and Figure 2 both show that including six transverse modes in the  $x$  direction produces a better representation of the  $a/b = 1$  panel displacement than does four.
3. Figure 3, like Figures 5 and 6 of Reference 1, shows that one transverse mode in the spanwise direction is not adequate for predicting the postflutter response and that two modes should be retained as a minimum.
4. This effort concludes that eight transverse modes in the  $x$  direction should be used for  $a/b = 2$  panels rather than the six stated in Reference 1. Figure 8 shows that the transverse results when incorporating eight modes in the flow direction is closer to the ten modes results than they are to the six modes results.
5. In Figure 8,  $\lambda_F$  decreases as the number of transverse modes in the  $x$  direction increases is different from Figure 8a of Reference 1, where  $\lambda_F$  increases with the increasing number of transverse  $x$  modes. (Recall that only one spanwise transverse mode was used in creating Figure 8a where two were used here.)
6. The general nature of the length-to-width flutter response comparison plot in Figure 11 compares well with the comparison in Figure 9 (Reference 1) although the number of



incorporated in-plane modes differs.

In-plane modal and time step convergence studies were performed on a simply supported panel so that comparisons could be made between this effort and previous work. The number of transverse modes used in each analysis was identical to the number of transverse modes used in each respective paper. The panel and flow parameters also match those in the compared paper if that information was provided.

Dowell investigated the nonlinear response of simply supported panels subject to supersonic flow over the upper surface in Reference 7. He determined the Airy stress function for the particular panel and flow parameters and then applied Galerkin's method to obtain the differential equation of motion that was then solved using a numerical time integration scheme. A first order expansion in reduced frequency of the exact two dimensional, unsteady, linearized, potential flow equation was incorporated to predict the quasi-steady aerodynamic loading. The maximum nondimensional transverse response versus nondimensional dynamic pressure at location  $(0.75a, 0.50b)$  for the simply supported panel created using the Rayleigh-Ritz method presented here is shown in Figure 43. The nondimensional dynamic pressure in this figure is defined as in Reference 7. The modal functions used to approximate the displacements are

$$\alpha_i(\bar{x}) = \phi_i(\bar{x}) = \sin(i\pi\bar{x})$$

$$\beta_j(\bar{y}) = \psi_j(\bar{y}) = \sin(j\pi\bar{y})$$

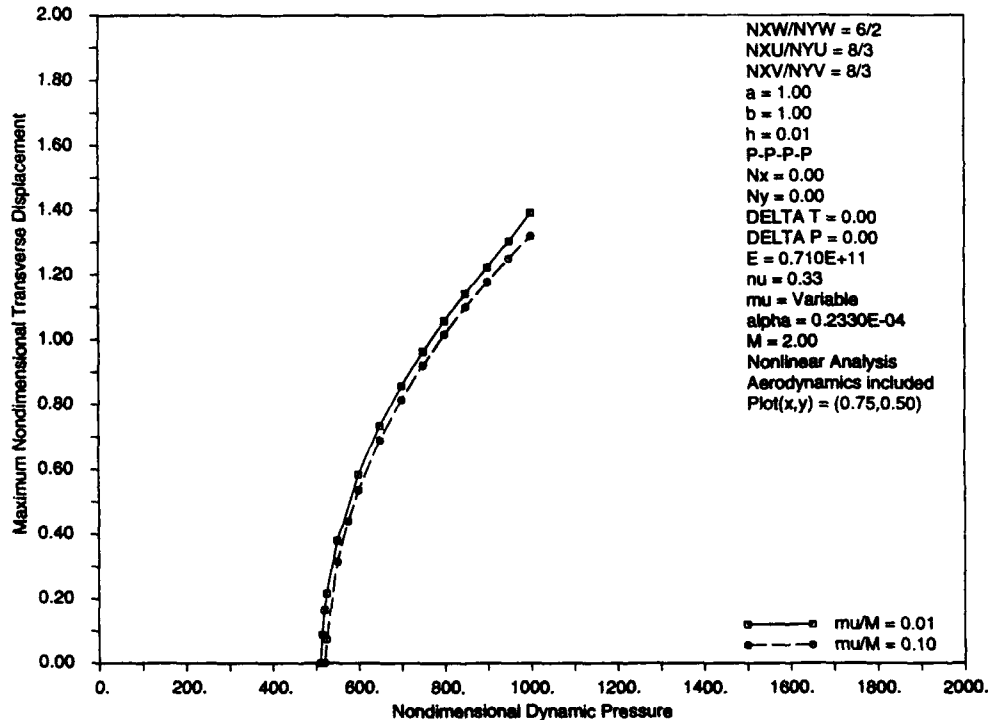


Figure 43 Plot comparing the steady state response of  $\mu/M = 0.01$  and  $\mu/M = 0.10$  panels.

The number of required in-plane modes determined in the convergence study is stated on the top right of the figure and the nondimensional time step used in creating the simply supported panel response plots was 0.001, one fifth of the time step used in determining the response of the cantilevered panels. The  $\mu/M = 0.01$  curve in Figure 43 appears to be identical to the same curve in Figure 16 of Reference 7. The flutter dynamic pressure predicted for the  $\mu/M = 0.10$  panel is lower than that predicted in Reference 7 and yet the response for  $\lambda \geq 600$  appears to be identical to that shown in Figure 16. Finally, the nondimensional flutter dynamic pressure for the  $\mu/M = 0.01$  panel in Figure 43 is 510.

The nondimensional dynamic pressure at which the simply supported panel in Reference 8 became unstable was  $\lambda \approx 512$  (the definition of  $\lambda$  in Reference 8 is the same as in Reference 7). Schaeffer and Heard used Galerkin's method to analyze a square panel whose boundaries were restricted such that the panel was simply supported in the transverse direction and unrestrained in-plane. Six modes were used to approximate the transverse displacement in the flow direction and two modes were used in the span direction. They used Ackeret's theory to determine the aerodynamic loads. This theory differs from first order piston theory in that the time dependence is neglected. The mass ratio used in determining the flutter dynamic pressure was not stated in this report. However, the predicted flutter dynamic pressure is within approximately 1 percent of the critical dynamic pressure predicted in Reference 7 and with this analysis when  $\mu/M = 0.01$ . A linear strain-displacement relation was used in this effort, so the postflutter onset response was not investigated.

Xue and Mei predicted the postflutter response of a simply supported panel using triangular and rectangular finite elements (Reference 9). They used the two dimensional, quasi-steady, aerodynamic theory employed in this effort and in References 1 and 7. The  $\Delta T/\Delta T_{cr} = 0.0$  curve in Figure 2 of their paper shows a comparison between their two finite element response results and Dowell's time domain results (Reference 7) where  $\mu/M = 0.10$ . Recall that the results using the analytical procedure outlined here for the same conditions are shown in Figure 43. The  $\mu/M = 0.10$  curve in Figure 43 is closest to the DKT element curve in Figure 2 of Reference 9. Note that the DKT element predicted the lower flutter dynamic pressure as well.

Reference 10 also investigated simply supported panels using a nonlinear strain-displacement model, except in their case, third order piston theory aerodynamics were incorporated. Bein, et. al., solved the panel governing equation following the same procedure as outlined in Reference 7. The maximum nondimensional transverse response versus nondimensional dynamic pressure for the fully simply supported panel at location  $(0.75a, 0.50b)$  is shown in Figure 44. This figure was created using the parameters stated in Table 1 of Reference 10. They are restated along the right side of the figure. The nondimensional dynamic pressure in this figure is defined as in Reference 10. The curve in Figure 44 appears to be identical to the first order piston theory curve in Figure 7 of Reference 10. Note that the second and third order piston theory curves in Figure 7 (Reference 10) show that the maximum steady state transverse response is dependent on the order of the aerodynamic theory under these conditions,  $M = 10$ . This differs from what Dowell stated in Reference 7 where he said the aerodynamic nonlinearity could be significant when  $Mh/a \sim O(1)$  because that ratio is about 0.1 when  $\lambda=800$ .

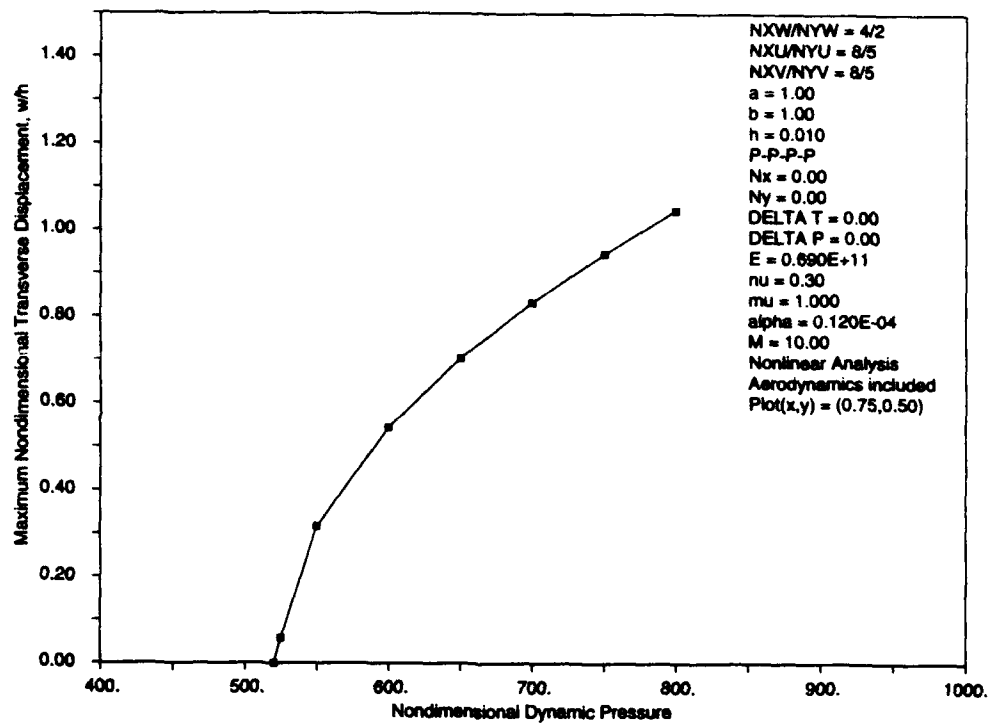


Figure 44 Maximum steady state response versus nondimensional dynamic pressure for a simply supported panel using the panel and flow parameters in Reference 10.

## SECTION V

### Conclusions

This effort investigated the postflutter response of a cantilevered panel subject to supersonic flow over the upper surface. Two length-to-width panels were studied, but the major emphasis was placed on the response of the square panel. It was shown that as the dynamic pressure was increased beyond the critical (flutter) dynamic pressure, the panel response shifted from a decay to  $z = 0$ , to a simple harmonic oscillation about  $z = 0$ , and then to a harmonic oscillation about some buckled position. Further increasing the dynamic pressure caused the panel to beat about a buckled position and then to oscillate sporadically. This sporadic oscillation occurs at approximately seven times the flutter onset conditions and has not been shown before for a panel without in-plane loads. It was shown also that the panel stretches in the cross-flow direction as it oscillates for all flow conditions greater than the critical conditions.

Convergence studies were performed on the nondimensional time step used in the time integration of the equations of motion and the number of in-plane and transverse modes employed in approximating the displacements. The modal convergence study indicates that the number of modes required to conduct a converged analysis is dependent on the length-to-width ratio of the panel. As the length-to-width ratio increases, the number of in-plane and transverse modes required increases. The square panel analysis used 28 modes to approximate both the  $x$  and  $y$  in-plane displacements and 12 modes to approximate the transverse displacement. As a comparison, the analysis of the panel whose length was twice its width used 32 modes to approximate the displacements in both the  $x$  and  $y$  directions and 16 modes to approximate the transverse displacement.

The response of the panel was studied by examining the displacement time histories, flutter mode shape, power spectral density, modified Poincaré, and phase plane plots at several dynamic pressures greater than the critical dynamic pressure. The primary modes influencing the postflutter onset response are the rigid body translation and rotation modes with the translation mode contributing five to ten times more than the rotation mode. The higher frequency structural modes contribute more as the flow conditions increase beyond the flutter onset conditions as shown in the figures. One sees the higher frequency contributions in the flutter mode shape figures where, for example, the free edges of the panel have more slope variations along them at  $\lambda = 640$  and  $700$  than when  $\lambda = 120$ . Also, the oscillation frequency increases as the flow conditions increase until the panel oscillates about some point other than  $z = 0$  after which the frequencies did not follow a smooth pattern.

The cantilevered panel results in this effort are compared with those in another paper that investigated the postflutter response of a cantilevered panel, Reference 1. A comparison of the postflutter response curves showed that the shape of the curves was essentially the same although the amplitudes differed. The number of transverse modes required to analyze a square panel was the same, but the number of transverse modes required to analyze a panel whose length is twice

its width differed. Also, the number of in-plane modes required to approximate the in-plane displacements were different for both panels only because an in-plane modal convergence study was performed here and not in Reference 1.

A panel with simple supports on all four sides was examined and compared to previously published results of the same panel boundary conditions. The analytical procedure followed throughout this effort produced results in excellent agreement with those of several different researchers that studied the panel using different analytical procedures (Galerkin method with time accurate and eigenvalue solutions, and finite element with a time accurate solution) and aerodynamic methods (piston and Ackeret's theories).

## **SECTION VI**

### **Acknowledgement**

The author would like to thank Dean Earl H. Dowell for the many valuable discussions concerning this effort. His ideas and encouragement are always welcome.

## SECTION VII

### Reference List

1. Weiliang, Y. and Dowell, E. H., "Limit Cycle Oscillation of a Fluttering Cantilever Plate," AIAA Journal, Volume 29, Number 11, November 1991, pages 1929-1936.
2. Hopkins, Mark A., "Nonlinear Equations of Motion for a Panel Subject to External Loads," WL-TM-93-308-FIBG, November 1993.
3. Dowell, E. H., "On Asymptotic Approximations to Beam Modal Functions," Journal of Applied Mechanics, Volume 51, June 1984, page 439.
4. Hopkins, Mark A., "Beam Modal Functions," WL-TM-92-339-FIBR, July 1992.
5. Press, W. H., et. al., Numerical Recipes, Cambridge University Press, New York, 1988, page 108.
6. Ketter, R. L. and Prawel, S. P., Modern Methods of Engineering Computation, McGraw-Hill Book Company, New York, 1969, page 274.
7. Dowell, E. H., "Nonlinear Oscillations of a Fluttering Plate," AIAA Journal, Volume 4, Number 7, July 1966, pages 1267-1275.
8. Schaeffer, H. G. and Heard, W. L., Jr., "Supersonic Flutter of a Thermally Stressed Flat Panel with Uniform Edge Loads," NASA TN D-3077, October 1965 (see also "Flutter of a Flat Panel Subjected to a Nonlinear Temperature Distribution," AIAA Journal, Volume 3, Number 10, October 1965, pages 1918-1923).
9. Xue, D. Y. and Mei, C., "Finite Element Nonlinear Panel Flutter with Arbitrary Temperatures in Supersonic Flow," AIAA Journal, Volume 31, Number 1, January 1993, pages 154-162.
10. Bein, T., Friedmann, P., Zhong, X. and Nydick, I., "Hypersonic Flutter of a Curved Shallow Panel with Aerodynamic Heating," paper presented at 34th AIAA Structures, Structural Dynamics and Materials Conference, April 19-22, 1993, La Jolla Ca.